Dynamical Trapping of Matter-Wave Bright Solitons in Optical Lattices

A Thesis

submitted to

Indian Institute of Science Education and Research Pune

in partial fulfillment of the requirements for the

BS-MS Dual Degree Programme

by

Ashutosh Misra

Indian Institute of Science Education and Research Pune

Dr. Homi Bhabha Road,

Pashan, Pune 411008, INDIA.

April, 2023

Supervisor: Dr. Rejish Nath

Certificate

This is to certify that this dissertation entitled Dynamical Trapping of Matter-Wave Bright Solitons in Optical Lattices towards the partial fulfilment of the BS-MS dual degree programme at the Indian Institute of Science Education and Research, Pune represents study/work carried out by Ashutosh Misra at Indian Institute of Science Education and Research under the supervision of Dr. Rejish Nath, Associate Professor, Department of Physics , during the academic year 2022-2023.

Dr. Rejish Nath

Committee:

Dr. Rejish Nath

Dr. Sebastian Wüster

This thesis is dedicated to my friends, family, and teachers, without whose constant love and motivation, accomplishing this body of work would have been unthinkable

Declaration

I hereby declare that the matter embodied in the report entitled Dynamical Trapping of Matter-Wave Bright Solitons in Optical Lattices are the results of the work carried out by me at the Department of Physics, Indian Institute of Science Education and Research, Pune, under the supervision of Dr. Rejish Nath and the same has not been submitted elsewhere for any other degree.

Ashutosh Misra

Acknowledgments

First and foremost, I would like to express heartiest gratitude to my supervisor, Dr. Rejish Nath, Department of Physics, IISER Pune, for providing treasured guidance and constant motivation through the formative years of my research experience. In the two years spent under his tutelage, I have been able to catch glimpses of his staggering work ethic and immaculate research etiquette which I shall diligently strive for in my own conduct as a researcher. Immense gratitude is owed to the imaginative culture of our research group, where testing out new things is highly encouraged and creative thoughts are carefully nurtured. I am grateful to fellow researchers Gautam, Inderpreet, Ratheejit, and Sandra for the several fruitful discussions with them regarding current and previous works which helped me in creating a unique amalgam of perspectives, ultimately coalescing to form an integral part of my thesis. Thanks are due to Dr. Sebastian Wüster for his insightful comments during the mid-year evaluation.

Sincere gratitude is extended to Dr. Diptimoy for giving an excellent opportunity to develop a taste for research early on and to Dr. Surjeet, Prof. Mahesh, Prof. Prasad, and Prof. Deepak Dhar for their dedication in conducting beautifully structured courses with thought-provoking discussions despite the COVID-19 pandemic, which piled onto my budding curiosity in plenty to pursue research in this field. Overall, I am indebted and grateful to the Department of Physics and the Indian Institute of Science Education and Research at Pune for providing the necessary resources, unwavering support, and a stress-free, quality environment to pursue my research. I am duly thankful to the Department of

Science and Technology, Government of India for providing financial support in the form of INSPIRE Scholarship for Higher Education (SHE) throughout the duration of my graduate studies.

I would like to convey my love and appreciation to all my friends who stuck with me throughout this journey and always provided unbridled support and motivation whenever it was needed. Finally, nothing would be possible without the unconditional love and affection of my parents and my dearest brother, on whom I could always fall back. Last but not the least, let me heartfully thank all those who have directly or indirectly contributed towards the completion of my research work.

Abstract

In this thesis, we investigate the dynamics of quasi-one-dimensional (Q1D) bright solitons in weakly coupled Bose-Einstein Condensates. The resulting dynamical regimes including Josephson-like oscillations and macroscopic quantum self-trapping (MQST) of solitons depend critically on the relative strengths of linear coupling and nonlinear interactions, mass imbalance, and the relative phase. We focus on a specific setup where bright soliton(s) traveling in a quasi-1D tube encounter a finite region where the coupling between the neighboring tubes is turned on, which leads to some very interesting dynamics. Depending on the shape of the coupling region, the initial velocity, and the dynamical regime, we observe dynamical trapping of the solitons within this coupling region. We characterize the nature of this trapping and describe the effective potential responsible using variational methods. We further propose an experimental setup for its realization and discuss the scope of applications of such trapping in experiments.

Contents

List of Figures

Introduction

The early work of S. N. Bose and A. Einstein laid the foundation for the theory of gas with indistinguishable particles of integer spins, which led to the discovery of a novel quantum phenomenon now called Bose-Einstein Condensation (BEC) [1, 2]. When the experimental observation of BECs was finally achieved after 70 years with the help of newly developed techniques in quantum optics [3, 4, 5], it led to a cascading emergence of unexpected avenues for new physics owing to the merger of atomic and optical physics [6]. Since then, ultra-cold atoms optics has emerged as a discipline in itself, capturing theoretical and experimental exploitation of an array of highly tunable quantum setups displaying extremely rich physics with extensive scope for applications.

Research on studying quantum gases in various trap geometries has gained a lot of importance owing to the precise control that can be achieved over its environment. Manipulation of coherent matter-wave solitons through external optical fields holds tremendous promise for applications in precision measurements using atomic interferometry and quantum information processing [6]. Not only that, but there is also scope for the development of quantum devices like atomic chips with bright solitons utilizing their scattering properties against barriers and enhanced phase sensitivity [7]. Moreover, the formation of bright solitons in optical lattices also opens up various paths for applications in building quantum simulators. With extensive control over its propagation in an external potential as well as its internal properties using techniques like Feshbach resonances, it has become increasingly possible to engineer a plethora of novel quantum technologies.

Tunneling between lattice sites or nonlinear interactions can be made space-dependent, which as we uncover in this study, can lead to a wide range of non-trivial physics. Dynamical localization in BECs can be seen using various techniques from disordered potentials to periodically driven lattices [8, 9]. In our case, we induce weak coupling between two Q1D tubes in a 2D optical lattice for a finite region and load a pair of moving bright solitons to study their dynamics on interaction with this region. We observe a dynamical potential leading to the localization of solitons depending on various parameters.

The thesis is structured in the following manner:

- **Chapter 1** : We explain the fundamental concept of Bose-Einstein Condensation and introduce its defining characteristics. We discuss the Hamiltonian in the mean-field approximation and the assumptions leading to quasi-1D bright solitons.
- **Chapter 2** : We overview the physics of BECs in optical lattices and introduce lattice approximations used in Wannier basis representation. We also briefly discuss the conditions for the collapse and decay of attractive condensates in traps.
- **Chapter 3** : We classify the dynamical regimes and the critical behavior of weakly coupled Q1D bright solitons through the mass imbalance and relative phase.
- **Chapter 4** : We investigate the dynamics of moving bright soliton(s) in the presence of a finite region with non-zero coupling. We characterize the dynamical confinement of the condensate within the coupling region and utilize a variational approach to understand the nature of the effective trapping potential.
- **Chapter 5** : We make final remarks on the results obtained and discuss its future scope.

Chapter 1

Bose-Einstein Condensation and Bright Solitons

1.1 Bose-Einstein Statistics

In this section, we look at the origin of Bose-Einstein condensation using the quantum statistical description developed by S. N. Bose and A. Einstein for non-interacting indistinguishable particles. We work in the grand canonical ensemble, where we can have an arbitrary number of particles in a given state, to make the interpretation much simpler. The probability of occurrence of a configuration in a gas with N' particles in a state k with energy E_k is given by $P_{N'}(E_k) = e^{-\beta(E_k - \mu N')}$. Here, μ is the chemical potential that fixes the overall particle number, and $\beta = 1/k_B T$ is the temperature.

For non-interacting bosons, we have an independent Hamiltonian for each particle and the resulting single-particle eigenstates allow unbounded occupation numbers in any of the states. Computing the full grand canonical partition function by summing over all possible

particle numbers, we are left with:

$$Z = \prod_i \frac{1}{1 - e^{-\beta(E_i - \mu N')}} \tag{1.1}$$

where E_i are the energy eigenstates of the single-particle states. We note here that for this sum to converge, we are required to assume that $E_k > \mu$ for all the states k. Similarly, for the ground state energy, $\mu < E_0$. Using the partition function, we now evaluate the average number of particles or number density:

$$\langle n_i \rangle = \frac{1}{e^{\beta(E_i - \mu)} - 1} \tag{1.2}$$

which is the Bose-Einstein distribution. This reduces to the familiar Boltzmann distribution in the limit of $(E - \mu)/k_B T >> 1$. We notice that when $\mu \to E_0$, the occupation number of the ground state diverges and becomes:

$$N_0 = \langle n_0 \rangle = \frac{1}{e^{\beta(E_0 - \mu)} - 1} \tag{1.3}$$

while for all the higher energy states, the thermal occupation number, $N_T = \sum_{i \neq 0} \langle n_i(\mu, T) \rangle$, increases for a given temperature T until it reaches a maximum cap of the critical occupation number N_c at $\mu = E_0$. This is the principle behind the macroscopic occupation of the ground state which we call Bose-Einstein condensation. Note that as T increases, $N_c(T)$ also increases, and when it goes beyond the total number of particles, $N_c(T) > N$, that temperature is called the critical temperature T_c and is defined as:

$$N_T \ (T_c, \mu = E_0) = N \tag{1.4}$$

Below this critical temperature, we can observe the phenomenon of Bose-einstein condensation. Let's consider a non-relativistic gas in a three-dimensional box of volume V. Then in the limit of very large N, one can replace the discrete energy spectra, $E = \frac{\hbar^2 k^2}{2m}$, with the

continuum approximation and get the density of states:

$$g(E) = \frac{V}{4\pi^2}\left(\frac{2m}{\hbar^2}\right)^{3/2} E^{1/2} \tag{1.5}$$

Here, since the lowest energy state is $E = 0$, μ is constrained to be negative. However, we carefully note that, as a result of the continuum approximation, $g(E)$ is proportional to $E^{1/2}$ and completely ignores the occupation of the $E = 0$ state. To rectify this omission, we write the occupation number as follows:

$$N = N_T + N_0 \tag{1.6}$$

where,

$$N_T = \frac{V}{4\pi^2}\left(\frac{2m}{\hbar}\right)^{3/2} \int \frac{E^{1/2}dE}{z^{-1}e^{\beta E} - 1} = \frac{V}{\lambda_T^3} g_{3/2}(e^{\beta\mu}) \tag{1.7}$$

and

$$N_0 = \frac{1}{z^{-1} - 1} = \frac{z}{1 - z} \tag{1.8}$$

where λ_T is the thermal wavelength and $z = e^{\beta\mu}$. The $g_{3/2}(z)$ is one of the classes of the Bose functions and for $z = 1$, it is equal to the Riemann zeta function, $g_n(1) = \zeta(n)$. Applying the condition given in (1.4), we arrive at the following expression for T_c:

$$T_c = \frac{2\pi\hbar^2}{mk_B}\left(\frac{n}{\zeta(3/2)}\right)^{2/3} \tag{1.9}$$

So, T_c for a gas in a 3D box depends entirely on the density of the gas. Combining the results from the expressions above for N_T and N_0, for $T < T_c$, we have:

$$\frac{N_0}{N} = 1 - \left(\frac{T}{T_c}\right)^{3/2} \tag{1.10}$$

Clearly, as $T \to 0$, more particles occupy the macroscopic ground state as it approaches the total number of particles. More particles added to the system for a fixed temperature go directly to the condensate fraction as the thermal cloud is already saturated.

1.2 One-Body Density Matrix and Order Parameter

1.2.1 Off-Diagonal Long-Range Order

After gaining an intuition from a microscopic perspective on how BECs come about, we turn to formalize the concept with the help of field operators. We obtain the one-body density matrix by tracing out the overall many-body density matrix and get:

$$\rho^{(1)}(\mathbf{r}, \mathbf{r}') \;=\; \langle \hat{\Psi}^\dagger(\mathbf{r}) \hat{\Psi}(\mathbf{r}') \rangle \tag{1.11}$$

where $\hat{\Psi}(\mathbf{r})$ and $\hat{\Psi}^\dagger(\mathbf{r})$ are the creation and annihilation operators, respectively, at the point $\mathbf{r}$. For a pure state, if the N-body wavefunction is given by $\Psi_n(\mathbf{r_1}, \mathbf{r_2}, ..., \mathbf{r_N})$, then the one-body density matrix can be evaluated by integrating over all the remaining degrees of freedom:

$$\rho_n^{(1)}(\mathbf{r}, \mathbf{r}') \;=\; N \int d\mathbf{r_2}\; d\mathbf{r_3} ... d\mathbf{r_N}\; \Psi_n^*(\mathbf{r}, \mathbf{r_2}, ..., \mathbf{r_N}) \Psi_n(\mathbf{r}', \mathbf{r_2}, ..., \mathbf{r_N}) \tag{1.12}$$

To evaluate this density matrix, we assume a spatially uniform and isotropic system of N particles in volume V and expand the field operators in terms of plane waves:

$$\hat{\Psi}(\mathbf{r}) = \frac{1}{\sqrt{V}} \sum_k \hat{b_\mathbf{k}} e^{i\mathbf{kx}} \tag{1.13}$$

where the annihilation and creation operators for bosons follow the commutation relations given by:

$$[\ \hat{b_{\mathbf{k}}}, \hat{b_{\mathbf{q}}}^{\dagger}\ ] \ = \ \delta(\mathbf{k}-\mathbf{q}) \tag{1.14}$$

With the help of the above, we can write the one-particle density matrix in the momentum basis as follows:

$$\langle\hat{\Psi}^{\dagger}(\mathbf{r})\hat{\Psi}(\mathbf{r}')\rangle = \frac{1}{V}\sum_{\mathbf{k},\mathbf{q}}\langle\hat{b_{\mathbf{q}}}^{\dagger}\hat{b_{\mathbf{k}}}\rangle e^{i\mathbf{k}\mathbf{r}-i\mathbf{q}\mathbf{r}'} \tag{1.15}$$

From the commutation relations, it can be derived that $\langle\hat{b_{\mathbf{q}}}^{\dagger}\hat{b_{\mathbf{k}}}\rangle$ is proportional to $\delta(\mathbf{k}-\mathbf{q})$. Treating the $\mathbf{k}=0=\mathbf{q}$ case separately, we have:

$$\rho^{(1)}(\mathbf{r},\mathbf{r}') \ = \ \frac{N_0}{V} + \sum_{\mathbf{k}\neq 0}\langle n_k\rangle e^{i\mathbf{k}(\mathbf{r}-\mathbf{r}')} \tag{1.16}$$

We gather from this expression that for $|\mathbf{r}-\mathbf{r}'|\to\infty$, the last term vanishes because of the rapidly oscillating complex exponential, and, as a result,

$$\rho^{(1)}(\mathbf{r},\mathbf{r}') \to \frac{N_0}{V} \qquad \text{as} \qquad |\mathbf{r}-\mathbf{r}'|\to\infty \tag{1.17}$$

The single-particle density matrix provides information about correlations between the basis states of the wave function. As larger $|\mathbf{r}-\mathbf{r}'|$ is reached, these correlations are usually expected to exponentially decay. However, as a result of the indistinguishability in the case of bosons housed in the commutation relations, the off-diagonal terms of this matrix do not vanish and saturate at a nonzero value, N_0/V. For $T<T_c$, as we have seen, there is a macroscopic occupation of this zero-momentum ground state and $\rho^{(1)}(|\mathbf{r}-\mathbf{r}'|)\to N_0/V$, which is finite and of the order of N/V over large distances. The system is said to possess an off-diagonal long-range order (ODLRO), which establishes coherence between atoms over a large spatial extent and allows them to migrate over long ranges without perturbing the system. This is a defining property of BECs.

1.2.2 Order Parameter

For interacting and non-uniform systems, instead of plane waves, we use the eigenfunctions of our Hamiltonian and write the field operators as:

$$\hat{\Psi}(\mathbf{r}) = \phi_0(r)\ \hat{b}_0 + \sum_{i\neq 0} \phi_i\ \hat{b}_i \tag{1.18}$$

where $\hat{b}_i$ are the annihilation operators for ϕ_i eigenstate. Here, we apply the *Bogoliubov Approximation*, where we replace the operators $\hat{b}_0$ and $\hat{b}_0^\dagger$ with the c-number $\sqrt{N_0}$. The reasoning for this comes from the macroscopic occupation of the $i = 0$ state, $N_0 >> 1$, and hence, the action of the creation or annihilation operator of a single particle in this ground state results in a negligible change in the state of the system. Moreover, we can combine the other $k \neq 0$ terms in one fluctuation term as $\delta\hat{\Psi}(\mathbf{r})$, and therefore, the field operator becomes $\hat{\Psi}(\mathbf{r}) = \sqrt{N_0}\phi_0 + \delta\hat{\Psi}(\mathbf{r})$.

We call the scalar term $\Psi_0 = \sqrt{N_0}\phi_0$ the "order parameter" of the system, as it encapsulates the transition to the macroscopically occupied GS in BECs for $T < T_c$. We also note the gauge freedom present in the choice of this order parameter, as the quantum state remains invariant on multiplication by a phase factor $e^{i\alpha}$. This is the U(1) gauge symmetry, which is spontaneously broken as we make an explicit choice of the phase and, hence, is the marker for the phase transition that leads to the formation of Bose-Einstein condensates.

1.3 Interacting Hamiltonian and Mean-Field Regime

In this section, we derive the mean-field equations for a weakly interacting system of condensates. We start by writing the full many-body interacting Hamiltonian in terms of

the field operators $\hat{\Psi}$:

$$\hat{H} = \int \left(\frac{\hbar^2}{2m} \boldsymbol{\nabla} \hat{\Psi}^\dagger \boldsymbol{\nabla} \hat{\Psi} + \hat{\Psi}^\dagger V_{ext}(\mathbf{r}) \hat{\Psi} \right) d\mathbf{r} + \frac{1}{2} \int \hat{\Psi}^\dagger \hat{\Psi}^{\dagger\prime} V(\mathbf{r}' - \mathbf{r}) \hat{\Psi} \hat{\Psi}' d\mathbf{r}' d\mathbf{r} \tag{1.19}$$

where $V_{ext}(\mathbf{r})$ is the external potential and $V(\mathbf{r})$ is the two-body interaction potential. We assume the two-body collisions to be short-range and isotropic and write them as:

$$V(\mathbf{r}' - \mathbf{r}) = g\delta(\mathbf{r}' - \mathbf{r}) \tag{1.20}$$

At low temperatures, only the s-wave scattering term stays relevant in the two-body potential. This is equivalent to an effective contact interaction potential with a given scattering length a_s, which we now write as:

$$V(\mathbf{r}' - \mathbf{r}) = \frac{4\pi\hbar^2 a_s}{m} \delta(\mathbf{r}' - \mathbf{r}) \tag{1.21}$$

Using the macroscopic occupancy of the GS in BECs, we replace the field operator with the order parameter Ψ. Further, after introducing contact interactions, we arrive at the well-known Gross-Pitaevskii equation:

$$i\hbar \frac{\partial \Psi}{\partial t}(\mathbf{r}, t) = \left(\frac{-\hbar^2}{2m} \boldsymbol{\nabla}^2 + V_{ext}(\mathbf{r}, t) + g \left| \Psi(\mathbf{r}, t) \right|^2 \right) \Psi(\mathbf{r}, t) \tag{1.22}$$

The Gross-Pitaevskii equation (GPE) describes the dynamics of a weakly interacting BEC within the mean-field approximation. It gives the time evolution of the order parameter Ψ subject to non-linear self-interaction. For $g > 0$, the interactions are repulsive, for $g < 0$, the interactions are attractive.

1.4 Reduced Dimensionality

With considerations regarding stability aside, BECs display highly manipulable experimental properties. Using a strong trapping potential, it is possible to dictate the shape of the condensate to a large extent and arrive at any desired geometry. In many cases, it is useful to have asymmetric condensate by employing an anisotropic external trapping potential. These anisotropies are often used to deform it into a *pancake* shape by taking $\omega_z > \omega_y, \omega_x$ or a *elongated cigar* shape by making $\omega_y, \omega_x > \omega_z$.

Given a sufficiently strong confinement, condensates in lower dimensions can even be realized. Consider $V(x, y, z) = \frac{1}{2}m(\omega_x^2 x^2 + \omega_y^2 y^2 + \omega_z^2 z^2)$ for which $\omega_y, \omega_x >> \omega_z$. It is possible to factor out the transverse part of $\psi(x, y, z)$ for this case and eliminate the extra degrees of freedom by assuming the wave function to be frozen in the GS of the strong harmonic trap in the xy plane. We can substitute this into the Gross-Pitaevskii equation and integrate over x and y to get the quasi-1D GPE:

$$\mu_{1D}\psi_z = \left(\frac{-\hbar^2}{2m}\frac{\partial^2}{\partial z^2} + \frac{1}{2}m\omega_z^2 z^2 + g_{1D}\left|\psi(z,t)\right|^2\right)\psi(z,t) \tag{1.23}$$

Here, we get $g_{1D} = \frac{g}{2\pi l_x l_y}$ and $\mu_{1D} = \mu - \frac{1}{2}\hbar(\omega_x + \omega_y)$. Condition on the validity of this approximation can be written as $\hbar(\omega_x\omega_y)^{1/2} >> \mu_{1D}$. We are left with a *cigar-shaped* tube of condensate, whose transverse degrees of freedom are frozen out.

Similarly, for the $\omega_y, \omega_x << \omega_z$ case, we end up with a *pancake-shaped* condensate, which has its d.o.f. along the z-axis eliminated. Note that, for studying the dynamics in condensates with reduced dimensionality, it is to be ensured that the validity condition on chemical potential always holds.

1.5 Q1D Bright Solitons in BECs

Without any external potential, the one-dimensional GPE is:

$$i\hbar\frac{\partial\psi}{\partial t} = -\frac{\hbar^2}{2m}\frac{\partial^2\psi}{\partial z^2} + g\left|\psi\right|^2\psi \tag{1.24}$$

This belongs to a class of equations referred to as the 1D Non-linear Schrodinger equations, which is encountered regularly when studying optics in non-linear media. It supports solutions called *solitons* which are non-linear localized wave packets that possess robustness against external perturbations. Their resistance to dispersion makes them ideal for use in communication media like optical fibers. They are called so because of their particle-like behavior in collisions.

Solitonic solutions for NLS equations are obtained using a technique called the inverse scattering transform. Depending on the sign of the interaction parameter g, dark solitons and bright solitons are supported. For $g > 0$ repulsive condensates, dark solitons are supported by the GPE which corresponds to a dip in the local density along with a phase jump across its middle. These also show particle-like behavior during collisions. For $g < 0$, when the interactions are attractive, the GPE supports solutions called *bright solitons*. These are peaks in local density and come about due to the self-trapping of the atoms against the dispersion. Their general form can be written as:

$$\psi(x,t) = \sqrt{\frac{k}{2}}\,\mathrm{sech}(k(x-ut))\exp[if(x,t)+i\phi] \tag{1.25}$$

where k characterizes the length scale depending on the interaction strength g, u and $f(x,t)$ determine the velocity, and ϕ is the complex global phase.

In this chapter, we have familiarized ourselves with the concept of Bose-Einstein Condensation and the mean-field equations governing the dynamics of interacting gas of BECs. We also looked at the conditions for realizing lower dimensional systems and their 1D solitonic

solutions. Now, we move on to study BECs in periodic potentials and various approximations involved for weakly interacting systems.

Chapter 2

Condensates in Optical Lattices

This chapter deals with the fundamentals of ultracold atoms in optical lattices. We give an overview of the light-matter interaction involved in generating a lattice potential using lasers. We write down the full many-body Hamiltonian and study it in the limit of weakly-interacting bosons. We give a brief outline of the dynamics in the case of repulsive atoms in periodic potentials before moving on to studying the attractive case.

2.1 Optical Lattice Potential

A periodic trapping potential that can hold Bose-Einstein condensates can be constructed using an interference pattern generated by counter-propagating laser beams. On interacting with an atom, the oscillating electric field induces a dipole moment in the atom, which now oscillates with the driving field. This dipole moment further interacts with the electric field to yield a dipolar potential as a result of the ac Stark shift seen in the atomic energy levels. We can write the energy shift or the dipolar potential as:

$$U_{dip} = -\frac{1}{2}\alpha(\omega)\langle E^2(\mathbf{r},t)\rangle \tag{2.1}$$

where $\alpha(\omega)$ is the polarizability depending on the driving frequency $\omega = \omega_{res} + \Delta$ and Δ is the detuning to the transition frequency, ω_{res}, for the atomic resonance. The time-averaged light intensity $I \propto |E(\mathbf{r})|^2$ of two identical counter-propagating laser beams, which appears in the above potential, creates an interference pattern with nodes and anti-nodes separated by half of the wavelength called the lattice spacing. The spatial modulation of the potential energy leads to a gradient force acting on the atoms such that they behave as if in a periodic lattice. Most experiments operate frequencies very close to the resonance where detuning $\Delta << \omega_{res}$ or the *rotating wave approximation* holds and the rapidly oscillating terms can be neglected. The sign of polarizability $\alpha(\omega)$ close to ω_{res} depends on whether the light is red-detuned ($\Delta < 0$) or blue-detuned ($\Delta > 0$), which decides whether the nature of the intensity peaks will be attractive or repulsive. In the general case with three pairs of counter-propagating beams, the spatial variation of the potential is given by:

$$V_{OL}(x, y, z) \;=\; V_0(\sin^2 kx + \sin^2 ky + \sin^2 kz) \tag{2.2}$$

Since the dipole force is derived from the gradient of this interaction potential, the force is conservative in nature. However, in the semiclassical case, we have the damping term that comes from the spontaneous decay of the excited state of the two-level system. Within this two-level approximation, if the decay rate due to spontaneous emission is Γ, then we can write the corresponding scattering rate as:

$$\Gamma_{sc} \propto \left(\frac{\Gamma}{\Delta}\right)^2 \tag{2.3}$$

In order to reach a conservative potential suitable for the dipolar trapping of condensates, we are interested in the far-detuned case to minimize scattering as much as feasible. Therefore, to realize such optical traps, experiments usually recommend keeping high intensities and large detunings.

It is extremely hard to understate the incredible amount of control and tunability offered

by optical trapping potentials on setups with ultracold atoms. From highly tunable lattice parameters to creating interesting lattice geometries in various models and state-dependent potentials using different polarization vectors, the possible extent of applications is vast (refer [10, 11] for a detailed review). In the next section, we look at one of such cases, i.e., the Hamiltonian of BECs in a lattice potential, and focus our study primarily on the weakly interacting case.

2.2 Hamiltonian

Starting with the many-body Hamiltonian for a gas of N interacting bosons, we approximate the two-body collisions by contact interactions given by $V(\mathbf{r}'-\mathbf{r}) = (4\pi a_s\hbar^2/m)\delta(\mathbf{r}'-\mathbf{r})$ to arrive at the Gross-Pitaevskii equation in the mean-field regime for a dilute gas:

$$i\hbar\frac{\partial\Psi}{\partial t}(\mathbf{r},t) = \left(-\frac{\hbar^2}{2m}\boldsymbol{\nabla}^2 + V_{OL}(\mathbf{r}) + g\left|\Psi(\mathbf{r},t)\right|^2\right)\Psi(\mathbf{r},t) \tag{2.4}$$

Consider a one-dimensional potential of the form:

$$V_{OL}(x) = V_0(\sin^2 kx) \tag{2.5}$$

where $k = \pi/L$. In accordance with the periodicity of the above potential, the condensate eigenfunctions can be written using Bloch's theorem:

$$\phi_{n,\mathbf{q}} = e^{i\mathbf{q}x}u_{n,\mathbf{q}}(x) \tag{2.6}$$

where $\mathbf{q}$ is the quasimomentum, n is the label for the energy band, and functions $u_{n,\mathbf{q}}(x+L) = u_{n,\mathbf{q}}(x)$ are periodic to allow expansion of the solution and potential in a Fourier series, all within the first Brillouin zone of the reciprocal lattice. Bloch functions form an orthogonal basis and the constituent condensate wavefunction is periodically extended over the entire lattice structure. The eigenfunctions and their energies depend on the depth of the lattice

potential V_0. In the context of a shallow lattice depth, Bloch functions are delocalized over the lattice and they give the exact band structure and the excitation spectrum using analytical and numerical methods. However, for a sufficiently deep lattice potential, energy scales are such that only the lowest-lying band is involved and the wavefunctions are highly localized at each site. To get a localized wavepacket in real space, a superposition of Bloch functions is used:

$$\phi_n(R, x) = \frac{1}{L} \int e^{-iRq} \Phi_{n,q}(x) \tag{2.7}$$

which is periodically translated using the phase factor e^{-iRq}, where R is the real-space lattice vector. This is equivalent to a change of basis, a unitary transformation from the Bloch states to a set of localized states called Wannier functions [12, 13, 14]. Unlike Bloch states, these give the localized wavefunctions at the center of each lattice site, which subsequently get translated to the other lattice sites. On performing this transformation, we exchange the localization in energy for the localization in space, and hence, WFs are not eigenstates of the Hamiltonian.

In the weakly interacting case, the spatial extent of Wannier states depends on the number of atoms in each lattice site. For a 1D lattice potential with strong transverse confinement, the ansatz can be factored as follows:

$$\psi(r, t) = \sqrt{N_T} \sum_n \psi_n(t) \Theta(\mathbf{r} - \mathbf{r}_n) \tag{2.8}$$

Introducing this to the GPE, we arrive at the well-known discrete non-linear Schrodinger equation (DNLSE):

$$i\hbar \frac{\partial \psi_n}{\partial t} = -K(\psi_{n-1} + \psi_{n+1}) + U|\psi_n|^2 \psi_n + \epsilon_n \psi_n \tag{2.9}$$

where K is the nearest neighbor tunneling term, ϵ_i is the on-site energy, and U is the non-

linear interaction term:

$$K = -\int d\mathbf{r}\left[\frac{\hbar^2}{2m}\boldsymbol{\nabla}\Theta_n.\boldsymbol{\nabla}\Theta_{n+1} + \Theta_n V_{OL}\Theta_{n+1}\right] \tag{2.10}$$

$$\epsilon_n = \int d\mathbf{r}\left[\frac{\hbar^2}{2m}(\boldsymbol{\nabla}\Theta_n)^2 + V_{OL}\Theta_n^2\right] \tag{2.11}$$

$$U = gN\int d\mathbf{r}|\Theta_n|^4 \tag{2.12}$$

By choosing an ansatz with a time-dependent particle number and phase at each site, the dynamics of the DNLSE have been extensively studied in [15]. In this thesis, our focus is mainly on condensates with attractive interactions, which are briefly discussed in the next section.

2.3 Collapse in Attractive BECs

A BEC in 3D with attractive interaction is unstable as it tends to coalesce infinitely to reach higher densities and eventually collapses on itself. This situation can be simply avoided by adding an external trap that stabilizes the system [16, 17]. Using the Gross-Pitaevkii equation, it has been predicted in multiple studies [18, 19], and verified experimentally [20, 21], that when the number of atoms N in a trapped BEC with negative scattering length exceeds a critical value N_{cr}, a singularity is born at the center of the trap where the collapse dynamics is triggered, similar to the uniform case in 3D. If $N < N_{cr}$, energy from the interatomic interactions is below the spacings of the trapping potential and the condensate slowly decays through quantum tunneling. The scattering length of atoms in BECs can be controlled via a magnetic field using Feshbach resonances and tuned such that the interaction strength changes value from positive to negative and provide estimates of the stability conditions. Many theoretical and experimental studies have obtained a value for N_{cr} for distinct geometries, including [22], which provide an estimate of N_{cr} for the cylindrically

symmetrical case. They characterize the relation between N_{cr}, the scattering length a_{sc} and the transverse scaling $a_{\perp}$ in the following form:

$$\frac{N_{cr}|a_{sc}|}{a_{\perp}} = k \tag{2.13}$$

As a result of strong transverse confinement, this condition demands that the atoms are frozen in the lowest transverse vibrational level and the interatomic interactions are negligible compared to the level spacings. This can serve as a reference for the implementation of quasi-1D cylindrical tubes described later in this thesis, since as previously discussed, BECs in reduced dimensions are realized through anisotropic traps and stipulate similar restrictions on N_{cr} and a_{sc} can be derived. Attractive condensates show extended bright solitons in one-dimensional optical lattices which have been studied in the mean field regime and compared with DMRG results for the Bose-Hubbard Hamiltonian [23, 24, 25], where the phase coherence is lost in condensate for strong interaction strengths and it destabilizes to a quantum superposition state instead.

Chapter 3

Bright Solitons in Q1D Coupled System

In this chapter, we investigate the dynamics of bright solitons in two uniformly coupled 1D tubes and characterize their distinct dynamical regimes. In each of these regimes, we study the effect of population imbalance and relative phase on the dynamics. We identify a control parameter to tune the competing quantum interactions that govern the transition between these regimes and show its dependence on the initial state. We use the understanding of the distinct nature of competing interactions to further explain the dynamics in the spatially dependent coupling case in Chapter 4.

3.1 Setup

In this section, we introduce the coupled setup and the equations governing its dynamics. We first initialize a 2D optical lattice potential in xy plane given by $V(x, y) = V_0 [\sin^2(kx) + \sin^2(ky)]$ and keep the z-axis free of any external confinement. We assume that the lattice potential is sufficiently strong such that we are in the tight-binding regime and macroscopic

wavefunction is given by Wannier states associated with the lowest energy band in the transverse plane. From the resulting set of Q1D cigar-shaped tubes, we focus our study on the dynamics of only two such weakly coupled tubes. The evolution of macroscopic condensate wavefunction, $\Psi(\mathbf{r},t)$, is governed by the 3D Gross-Pitaevskii equation, given as:

$$i\hbar\frac{\partial\Psi(\mathbf{r},t)}{\partial t} = \left[-\frac{\hbar^2\nabla^2}{2M} + g_0|\Psi(\mathbf{r},t)|^2 + V(x,y)\right]\Psi(\mathbf{r},t) \tag{3.1}$$

where $g_0 = 4\pi a_{sc}\hbar^2 N/M$ characterizes the short range contact interaction with a_{sc} being the s-wave scattering length. In this thesis, we consider only attractive short-range interactions ($a_{sc} < 0$). In the tight binding regime, we can factorize the wavefunction at each lattice site and write it as a sum of localized Wannier basis states as:

$$\Psi(\mathbf{r},t) = \sum_{ij}\Psi_{i,j}(\mathbf{r},t) = \sum_{ij} w_{i,j}(x,y)\psi_{i,j}(z,t) \tag{3.2}$$

Using this ansatz (3.2) in the 3D GPE (3.1) and applying the weak coupling approximation described in [15], we obtain the discrete non-linear Schrodinger equation (DNLSE) given by:

$$i\hbar\frac{\partial\psi_{i,j}}{\partial t} = -\frac{\hbar^2}{2M}\frac{\partial^2\psi_{i,j}}{\partial z^2} + g_{1D}|\psi_{i,j}|^2 - J\left[\psi_{i+1,j} + \psi_{i-1,j} + \psi_{i,j+1} + \psi_{i,j-1}\right] \tag{3.3}$$

where,

$$J = -\iint dx\ dy\ w^*_{i,j}(x,y)\left[-\frac{1}{2}\left(\frac{\partial^2}{\partial x^2} + \frac{\partial^2}{\partial y^2}\right) + V(x,y)\right]w_{i+1,j}(x,y)$$

and $g_{1D} = g_0\iint dx\ dy\,|w_{i,j}(x,y)|^4$. Since we are considering only two such coupled 1D tubes, our equations reduce to:

$$\begin{aligned} i\hbar\frac{\partial\psi_1}{\partial t} &= -\frac{\hbar^2}{2M}\frac{\partial^2\psi_1}{\partial z^2} + g_{1D}|\psi_1|^2\psi_1 - J\psi_2 \\ i\hbar\frac{\partial\psi_2}{\partial t} &= -\frac{\hbar^2}{2M}\frac{\partial^2\psi_2}{\partial z^2} + g_{1D}|\psi_2|^2\psi_2 - J\psi_1 \end{aligned} \tag{3.4}$$

We place a single ground state bright soliton in each of the two tubes with no spatial offset in the z-direction, with the initial states given by:

$$\psi_j(z) = \frac{N_j\sqrt{|g_{1D}|}}{2}\,\mathrm{sech}\left(\frac{N_j|g_{1D}|z}{2}\right)\; e^{i\phi_j} \tag{3.5}$$

and the total number of atoms in both sites is fixed to $N_T = N_1 + N_2$. An initial constant phase difference, $\phi_0 = (\phi_1 - \phi_2)$, and/or a mass imbalance, $p_0 = N_1 - N_2$, can now be added between the two solitons in order to trigger non-trivial dynamics between the two sites. We run numerical simulations of (3.4) with the above ansatz for different values of J, p_0, and ϕ_0 and study the dynamics of the system.

3.2 Stationary States

First, we find the stationary points of the coupled system and look at their stability. This will later help us understand the dynamics arising due to deviation from these equilibrium states. We first make the (3.4) dimensionless by rescaling the variables and arrive at:

$$\begin{aligned} i\frac{\partial\psi_1}{\partial t} &= -\frac{1}{2}\frac{\partial^2\psi_1}{\partial z^2} + g_{1D}|\psi_1|^2\psi_1 - J\psi_2 \\ i\frac{\partial\psi_2}{\partial t} &= -\frac{1}{2}\frac{\partial^2\psi_2}{\partial z^2} + g_{1D}|\psi_2|^2\psi_2 - J\psi_1 \end{aligned} \tag{3.6}$$

where $g_{1D} \to \frac{g_{1D}Mb}{\hbar^2}$, $J \to \frac{JMb^2}{\hbar^2}$ and b is the lattice spacing. We can derive the above coupled GPEs from the Lagrangian given by:

$$L(t) = \int_{-\infty}^{\infty}\left\{\sum_j\left[\frac{i}{2}\left(\psi_j^*\frac{\partial\psi_j}{\partial t} - \psi_j\frac{\partial\psi_j^*}{\partial t}\right) - \frac{1}{2}\left|\frac{\partial\psi_j}{\partial z}\right|^2 + \frac{|g_{1D}|}{2}|\psi_j|^4\right] + J(\psi_1^*\psi_2 + \psi_1\psi_2^*)\right\}dz \tag{3.7}$$

We input the GS ansatz from (3.5) into the above Lagrangian and evaluate the integral to obtain the following:

$$L(t) = -[\dot{\phi_1} N_1 + \dot{\phi_2} N_2] + \frac{|g_{1D}|^2}{24} [N_1^3 + N_2^3] + \frac{4J}{N_T} N_1 N_2 I(p) \cos(\phi) \tag{3.8}$$

where we have defined mass imbalance as $p(t) = (N_1 - N_2)/N_T$ and phase difference as $\phi = (\phi_1 - \phi_2)$. The integral $I(p)$ cannot be solved analytically and is given by:

$$I(p) = \int_0^\infty \frac{dz}{\cosh^2(z) + \sinh^2(pz)} \tag{3.9}$$

On solving the Euler-Lagrange equations for $p(t)$ and $\phi(t)$, we get these time evolution equations:

$$\begin{aligned} \dot{p} &= (1 - p^2) I(p) \sin(\phi) \\ \dot{\phi} &= -\Lambda p - \cos(\phi) \frac{d}{dp} [(1 - p^2) I(p)] \end{aligned} \tag{3.10}$$

where t is rescaled by a factor of $2J$ and

$$\Lambda = \frac{(|g_{1D}| N_T)^2}{16J} \tag{3.11}$$

By putting the time derivatives in the LHS of (3.10) equal to zero, we get the following stationary states:

$$\begin{aligned} \phi_0 &= 0, & p_0 &= 0 \\ \phi_0 &= \pi, & \Lambda p_0 &= I'(p_0)(1 - p_0^2) - 2 p_0 I(p_0) \\ \phi_0 &= \cos^{-1}\left[\frac{2\Lambda}{\pi}\right], & p_0^2 &= 1 \end{aligned} \tag{3.12}$$

On performing linear stability analysis by adding small perturbations to the above stationary states, we obtain the following information about their stability. For $\phi_0 = 0$ and $p_0 = 0$, we start with identically distributed atoms in both the two tubes with no initial phase difference.

This is a stable fixed point as we get sinusoidal solutions for small fluctuations in $p(t)$ and $\phi(t)$. For the π-phase stationary point, small fluctuations lead to distinct unsteady states depending on the value of Λ and, hence, it is an unstable fixed point. The third stationary state only exists when $\Lambda < \pi/2$. For such values of Λ, the fixed point is always unstable since any small perturbation in the $\phi(t)$ and $p(t)$ leads to a periodic transfer of atoms between the two tubes. Note that the dynamical parameter Λ above decides the stability of the stationary states and is therefore key in understanding the dynamics obtained from non-equilibrium initial states studied in the next section.

3.3 Self-Trapping and Switching Dynamics

We start with a pair of bright solitons, one in each tube, linearly coupled with each other via the lattice potential. We numerically simulate (3.4) using the Split Step Method (SSM) for the diagonalized Hamiltonian. It should be noted here that we only start with the GS sech form of the wavefunction given in (3.5) and the SSM allows it to take any waveform during its time evolution, allowing for higher excitations to emerge. For this scenario, we observe different dynamical regimes based on $\Lambda = \frac{(gN_T)^2}{16J}$, which represents the relative strength of the contact interactions and tunneling strength, for a varying extent of initial asymmetry between the solitons. We divide the results into three cases around the critical value Λ_c:

- $\Lambda << \Lambda_c$: Switching
- $\Lambda \lessapprox \Lambda_c$: Non-periodic Transfer
- $\Lambda > \Lambda_c$: Self-Trapping

To change the value of Λ, we can either (i) modify the overlap between the transverse atomic clouds of the two condensates by changing the lattice depth V_0 or the spacing between the tubes or (ii) change the number of atoms in the condensate. Here, we assume that the weak

coupling approximation used to derive (3.4) still holds, where the non-linear interactions in the inter-layer overlap are weaker than the nonlinear self-interactions within each layer.

3.3.1 $\Lambda << \Lambda_c$: Switching

For $\Lambda = 0.31 << \Lambda_c$, we start with an out-of-equilibrium initial state by providing an asymmetry in the mass and the phase of the solitons. In this high coupling limit, for a single soliton loaded in one tube, $p_0 = 1$, and $\phi_0 = 0$, we see periodic Rabi-like oscillations in the population difference between the tubes with a frequency of $\omega_R \approx 2J$. Here, $p(t)$ oscillates around $p = 0$ between $p = \pm 1$. This is called complete or perfect switching as the entire mass of the soliton migrates from one layer to the other during the oscillations. When $p_0 = 0.6$ or any $0 < p_0 < 1$ and $\phi_0 = 0$, the soliton switches incompletely between the tubes as $p(t)$ still oscillates around $p = 0$ but with an amplitude of approximately $p_0 < 1$. Figure (3.1) (a) and (b) show the density evolution in each of the tubes and figure (3.2) gives the plots for mass difference $p(t)$ during the dynamics.

Providing an asymmetry via an initial phase difference also leads to similar dynamics. For $p_0 = 0$ and $\phi_0 = \pi/2$, the soliton switches completely and periodically oscillates between $p = \pm 1$ while for $\phi_0 = \pi/4$, the switching is incomplete. Figure (3.3) (a) and (b) give the density plot for $\phi_0 = \pi/2$. This mass flow can be better understood using the hydrodynamic description of BECs [16]. The phase difference given in the transverse direction is interpreted as an initial nonzero superfluid velocity towards the increasing phase.

Periodic oscillations in the density arise from the linear coupling between the tubes. Here, we operate in the non-interacting limit where the non-linear effects of contact interactions are negligible. So, in the absence of interactions, atoms in the condensate tend to coherently tunnel between the two tubes. We note that for $0 < \Lambda << \Lambda_c$, very small excitations emerge around the central solitonic waveform during each oscillation which can be attributed to the nonlinearity present in the system. However, they have a negligible impact on the dynamics

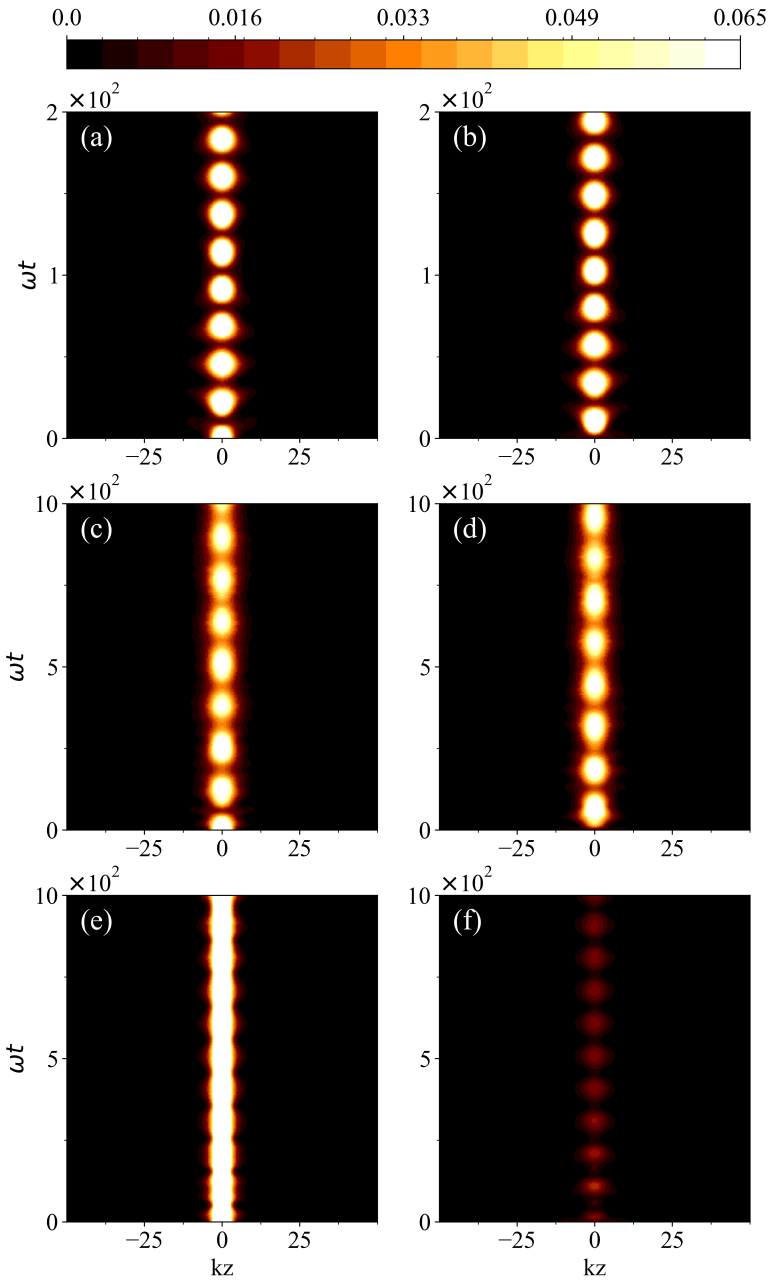

Figure 3.1: Dynamics of two linearly coupled bright solitons in Q1D tubes with an initial mass difference $p_0 = 0.6$ between them for $g_{1D} = -1$. The density evolution given in each row corresponds to a system of two coupled Q1D tubes and colorbar on top gives the density scale for all. $\Lambda = 0.31$ in (a) and (b), mass asymmetry leads to coherent population transfer oscillations between the solitons with $\langle p \rangle = 0$. $\Lambda = 1.25$ in (c) and (d), atomic flow yields non-periodic oscillations in density around $\langle p \rangle \approx 0$. In (e) and (f), $\Lambda = 2.08$, the direction of flow gets reversed and condensate gets self-trapped with $\langle p \rangle \neq 0$ in the tube with larger initial mass.

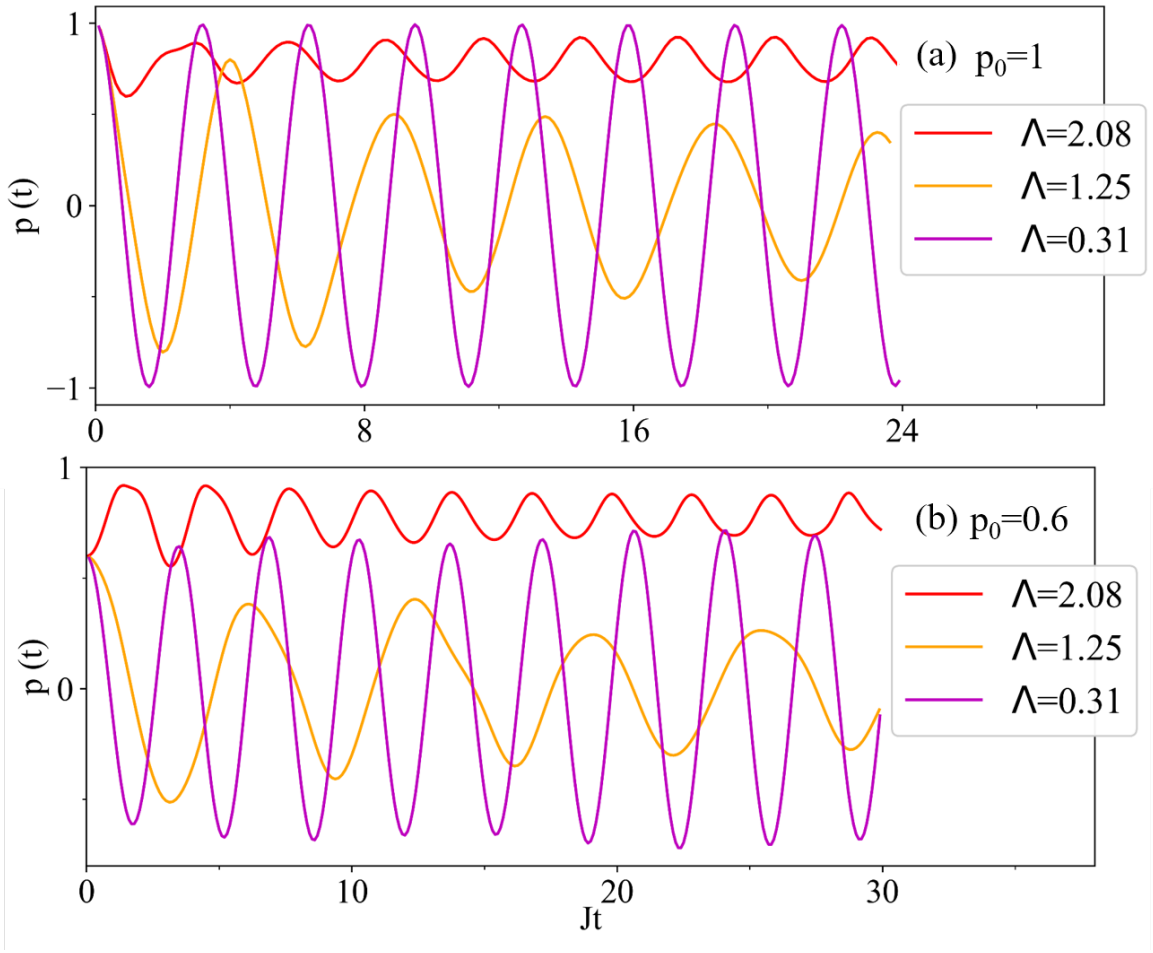

Figure 3.2: Population difference $p(t)$ with rescaled time Jt for $\phi_0 = 0$ and (a) $p_0 = 1$ and (b) $p_0 = 0.6$; For both cases (a) and (b): $\Lambda = 0.31$ leads to switching dynamics, $\Lambda = 1.25$ leads to non-periodic population transfer, $\Lambda = 2.08$ leads to self-trapping

and can be safely ignored.

3.3.2 $\Lambda \lessapprox \Lambda_c$: Non-periodic Transfer

On increasing $\Lambda \lessapprox \Lambda_c$, oscillations in $p(t)$ become non-periodic but are still around the average $\langle p(t) \rangle \approx 0$. The amplitudes of the oscillations are also reduced. As J is smaller than before for a fixed g in this case, the time period of the oscillations increases. This can be seen from Figures (c) and (d) in (3.1) where $p_0 = 0.6$ and in (3.3) where $\phi_0 = \pi/2$ and the mass imbalance plots in (3.2) and (3.4). Since the interactions are non-linear and attractive, they provide a self-focussing tendency to condensate and lend an anharmonic character to the oscillations. We see that nonlinear interactions disrupt the periodicity of these oscillations analogous to the dynamics of a non-rigid pendulum where the initial mass imbalance corresponds to the initial angular momentum [26, 27]. It should be noted that due to the increase in relative non-linearity, peripheral excitations around the soliton get slightly bigger, however, still are negligible enough to substantially impact the dynamics for the time scales considered.

Due to the spatial freedom afforded to the wavefunction along the tube axis with respect to its waveform, we do not observe a critical slowing down of the dynamics at Λ_c as seen in [26, 28, 27], where $p(t)$ decays to 0. Instead, a mixture of behaviors from both the dynamical regimes from below and above Λ_c is seen as we approach closer, and hence, a sharp border cannot be determined for $\Lambda = \Lambda_c$. We choose to identify Λ_c based on the value of $\langle p(t) \rangle$, averaged over a reasonable time scale depending on J, as we vary Λ. Plots for these are explained in section 3.4.

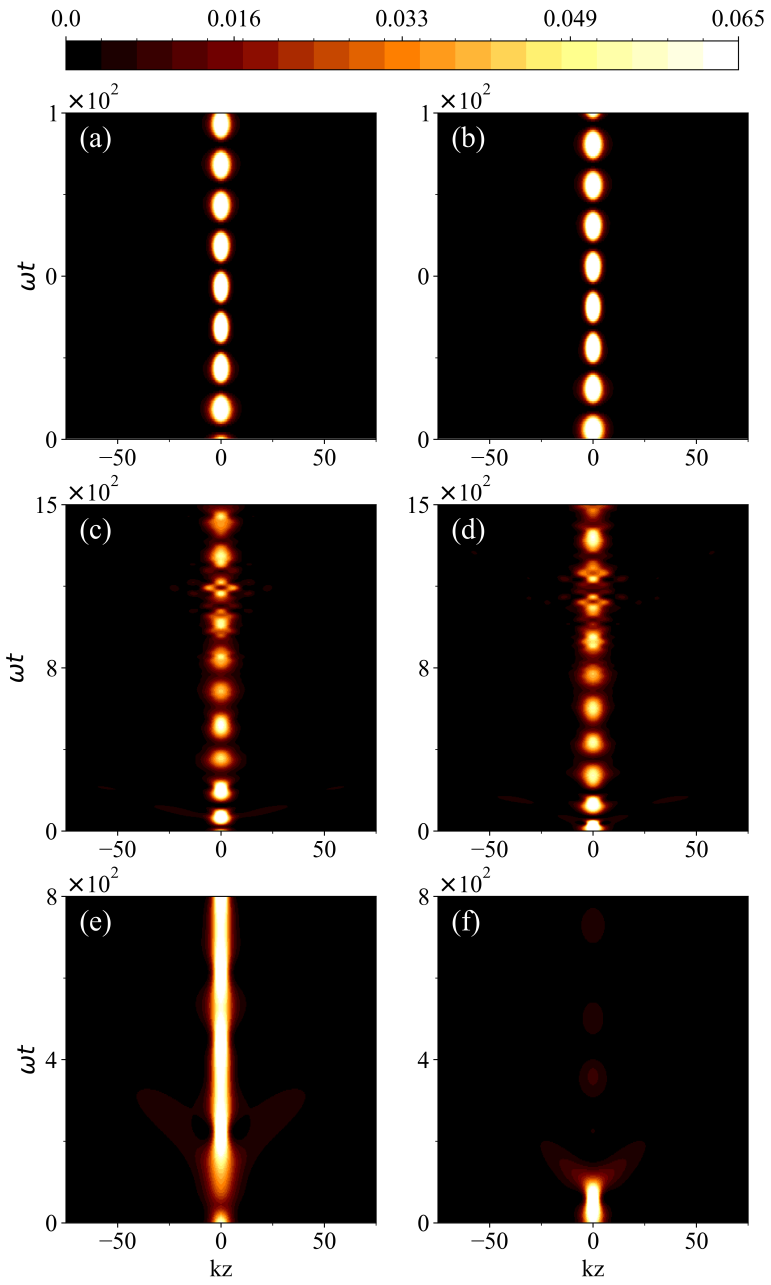

Figure 3.3: Dynamics of two identical coupled bright solitons in Q1D tubes with an initial phase difference $\phi_0 = \pi/2$ between them for $g_{1D} = -1$. The density evolution given in each row corresponds to a system of two coupled Q1D tubes and colorbar on top gives the density scale for all. $\Lambda = 0.25$ in (a) and (b), phase gradient leads to coherent population transfer oscillations between the solitons with $\langle p \rangle = 0$. $\Lambda = 2.0$ in (c) and (d), non-periodic oscillations in density around $\langle p \rangle \approx 0$ takes place. In (e) and (f), $\Lambda = 6.25$, condensate gets self-trapped with $\langle p \rangle \neq 0$ in the tube opposite to the direction of initial atomic flow. Note the initial direction of flow stays the same for all three cases.

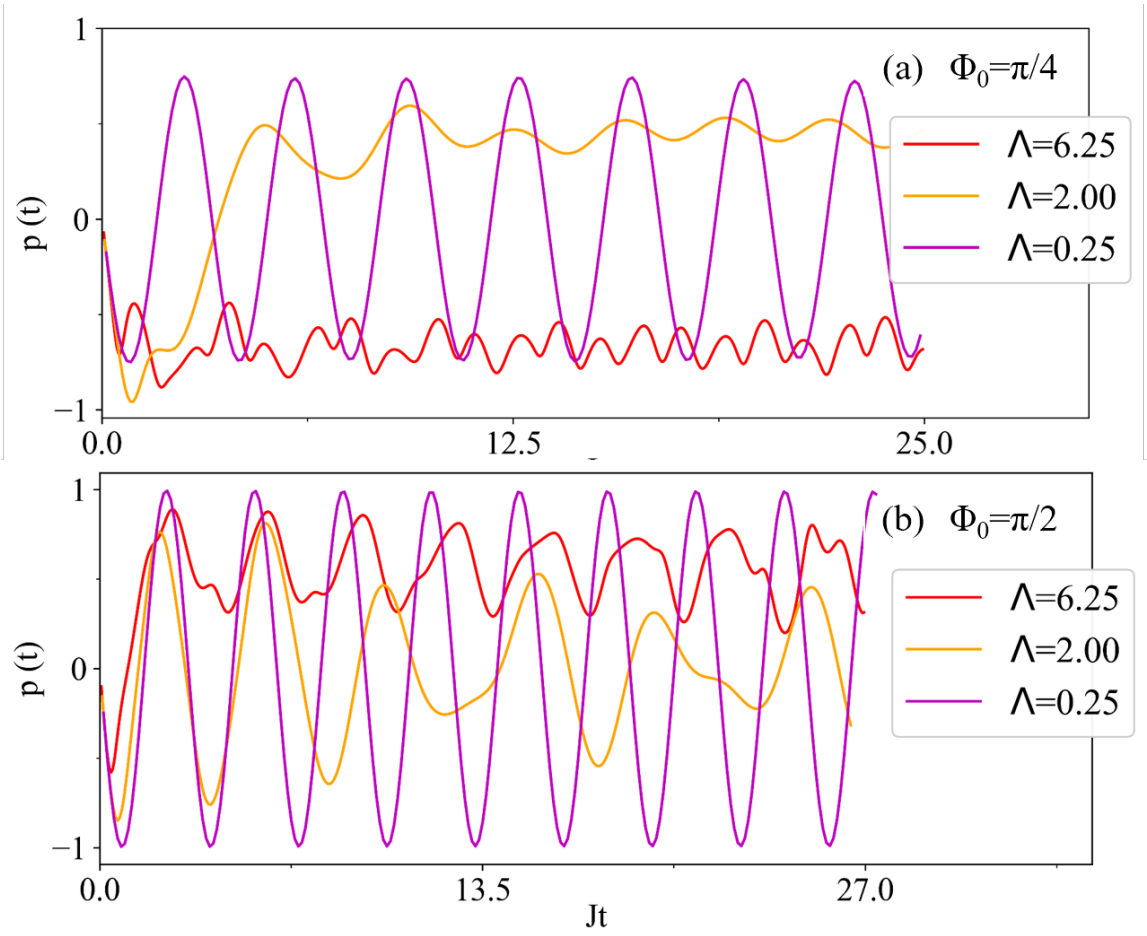

Figure 3.4: Population difference $p(t)$ with rescaled time Jt for $p_0 = 0$ and (a) $\phi_0 = \pi/4$ and (b) $\phi_0 = \pi/4$; For both cases (a) and (b): $\Lambda = 0.25$ leads to switching dynamics, $\Lambda = 2.0$ leads to non-periodic population transfer, $\Lambda = 6.25$ leads to self-trapping, however, in different tubes in spite of the same direction of initial flow.

3.3.3 $\Lambda > \Lambda_c$: Self-Trapping

As we further increase Λ beyond a certain threshold, the mass imbalance starts to oscillate non-periodically around a non-zero $\langle p \rangle \neq 0$ with a small amplitude, as shown in Figure (3.1) and (3.3). This is called macroscopic quantum self-trapping (MQST) which results from the nonlinearity of the contact interactions within the condensate. The nonlinear interactions counter the tendency of the condensate atoms to tunnel coherently to the neighboring tube. For $\Lambda = 2.08$ and $p_0 = 1$, a small fraction of the soliton's mass tunnels to the other tube, and a larger fraction stays in the initial tube, resulting in small oscillations around $\langle p \rangle = 0.79$, whereas, for $p_0 = 0.6$, mass instead flows from the tube with the smaller soliton mass to the other, finally oscillating about $\langle p \rangle = 0.77$ (see fig. 3.2). When $p_0 = 0$ and $\phi_0 = \pi/2$, self-trapping is seen for a larger value of $\Lambda = 6.25$ due to the dependence of Λ_c on the initial conditions.

We note that while the value of ϕ_0 or p_0 decides the direction of the initial mass flow between the tubes, we cannot predict which tube the condensate will eventually get self-trapped in, which can be seen from Figure (3.2) and (3.4). Due to this unpredictability, it becomes difficult to engineer applications involving controlled "atomic switching" of solitons using these coupled tubes to mimic the behavior seen in directional fiber couplers [29].

On increasing Λ further, we risk losing the validity of the mean-field approximation and the weak coupling limit as quantum fluctuations come into play to describe the dynamics accurately.

3.4 Dependence of Λ_c on Initial State

The dynamics of this weakly coupled system of BECs with non-linear interactions can be understood using some analogies in classical mechanics. It has been stated in previous works

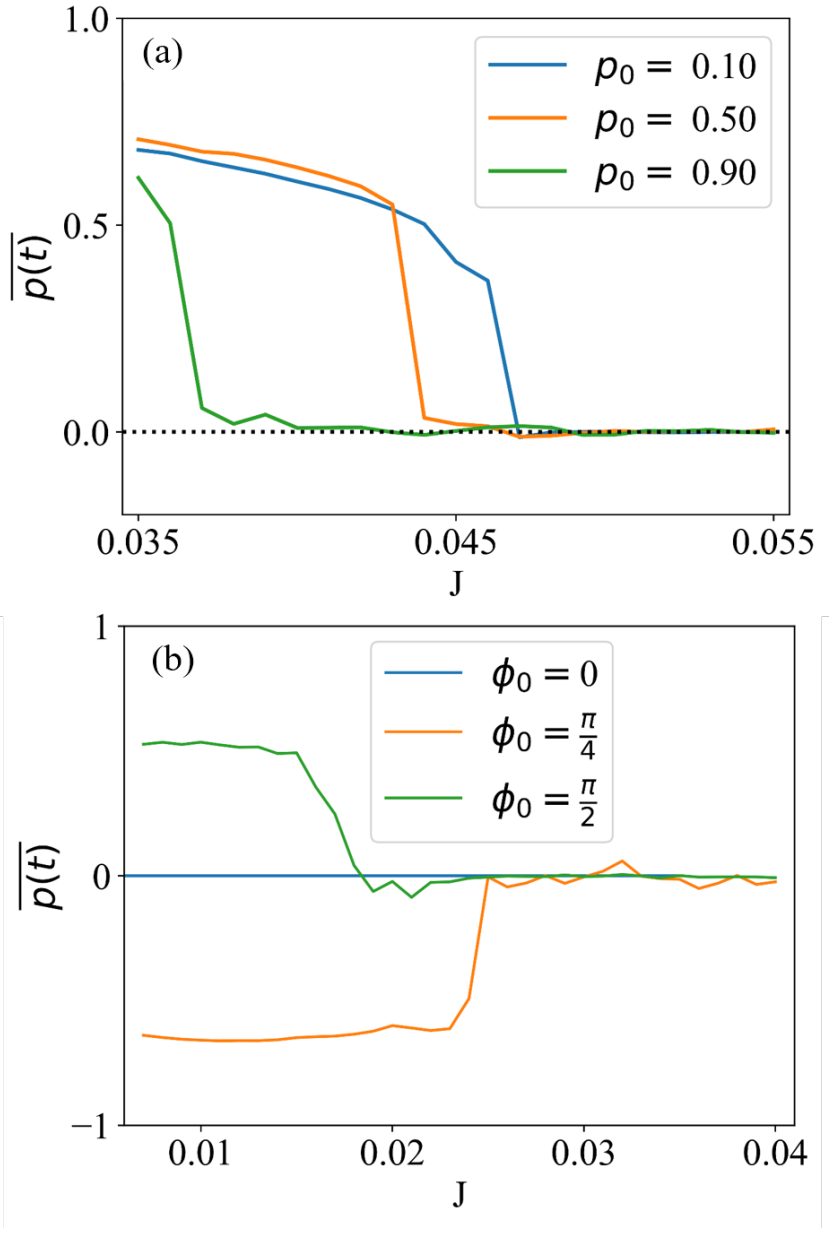

Figure 3.5: $\langle p \rangle$ vs J for varying asymmetry in (a) p_0 and (b) ϕ_0. Transition from $\langle p \rangle \neq 0$ to $\langle p \rangle \approx 0$ marks J_c corresponding to Λ_c for $g_{1D} = -1$. Λ_c increases (a) from $\Lambda_c = 1.33$ for $p_0 = 0.1$ to $\Lambda_c = 1.69$ for $p_0 = 0.9$ and (b) from $\Lambda_c = 2.5$ for $\phi_0 = \pi/4$ to $\Lambda_c = 3.47$ for $\phi_0 = \pi/2$.

[26, 27] that the dynamical scenarios observed in such systems correspond to the dynamics of a non-rigid pendulum in a plane, where $p(t)$ is the angular momentum, ϕ is the tilt angle to the vertical, and $\sqrt{1-p^2}$ is the length of the pendulum. The parameter Λ, the measure of non-linearity to linearity here, can be mapped to the inverse of the moment of inertia of the pendulum. This governs the critical transition from the switching to the self-trapped case.

The oscillations which occur about $p \approx 0$ can be represented by the case where the pendulum isn't provided with sufficient kinetic energy to overcome the potential fence corresponding to the bob at the "π position" and thereafter slows down to halt before changing its direction of motion and oscillating so forth. The smaller the amplitude of p_0, the more periodic the oscillations. When the kinetic energy or p_0 is sufficient to overcome the potential barrier, the bob crosses over the "π position", avoids the zero angular momentum state $p = 0$, and instead performs rotations about some $p \neq 0$. This corresponds to the self-trapped case where there is a perpetual mass imbalance and the relative phase runs abound.

We note that the potential barrier peak at $\phi = \pi$ must depend on the value of the moment of inertia. Moreover, the initial energy given through both p_0 and ϕ_0 dictates how the length of the non-rigid pendulum evolves, and hence, is also a key factor in deciding the height of the potential's peak. Therefore, to obtain a critical value p_c or ϕ_c for which the bob crosses the "π position", with the help of energy conservation, we obtain an expression that depends on Λ [28]. So, for a given Λ, there exists a critical initial asymmetry given through p_c or ϕ_c, which will mark the transition from switching to the self-trapped case. Equivalently, it can be asserted that for a given p_0 and ϕ_0, there exists a critical value Λ_c marking the same transition. We study the variation in Λ_c for different initial conditions through time averaged p. Figure (3.5) gives this time-averaged value of p as a function of J or Λ obtained through the numerical simulation of the GPE (3.4). Λ_c is identified from the value of J where $\langle p(t) \rangle \approx 0$. We note that Λ_c increases with the extent of asymmetry in the

initial state, both through mass and phase difference.

In summary, the dynamics of two weakly coupled bright solitons in Q1D tubes show a critical dependence on Λ exhibiting a transition from coherent switching to macroscopic self-trapping dynamics. The different regimes are manifest in the average population imbalance wherein for the switching case $\langle p \rangle \approx 0$, which differs from the self-trapped case where $\langle p \rangle \neq 0$. Further, we look at the dependence of the critical parameter on the initial conditions and explain it in analogy with the classical non-rigid pendulum.

Chapter 4

Dynamical Confinement

Randomness and disorder are ubiquitously found in physical systems in the form of defects and impurities, which typically trigger dispersive processes throughout the system, thus, disrupting any meaningful dynamics. This naturally generates interest in finding systems where these diffusive tendencies are negated and the order can be maintained through localization in energy and space. Localization can be defined as a concentration of energy or probability density in a finite region of space against diffusive tendencies. In a major breakthrough, P.W. Anderson (1958) discovered a counter-intuitive phenomenon of strong localization arising in a disordered quantum system such that given enough disorder, no diffusion takes place [8]. Since then, from solitons in external traps and periodically driven lattices to disordered quantum setups, many studies focus their search on novel quantum phenomena that allow for control and flexibility over the dynamics through localization and many have made major headway.

In this chapter, we introduce a setup with a spatially dependent coupling parameter, $J(z)$, in coupled Q1D tubes and study the dynamics as a single or a pair of moving bright solitons interact with this coupling region. We observe dynamical confinement of solitons inside this region as it gets localized spatially. We employ a variational approach to explain

the resulting dynamics and obtain an effective potential for $J(z)$.

4.1 Setup

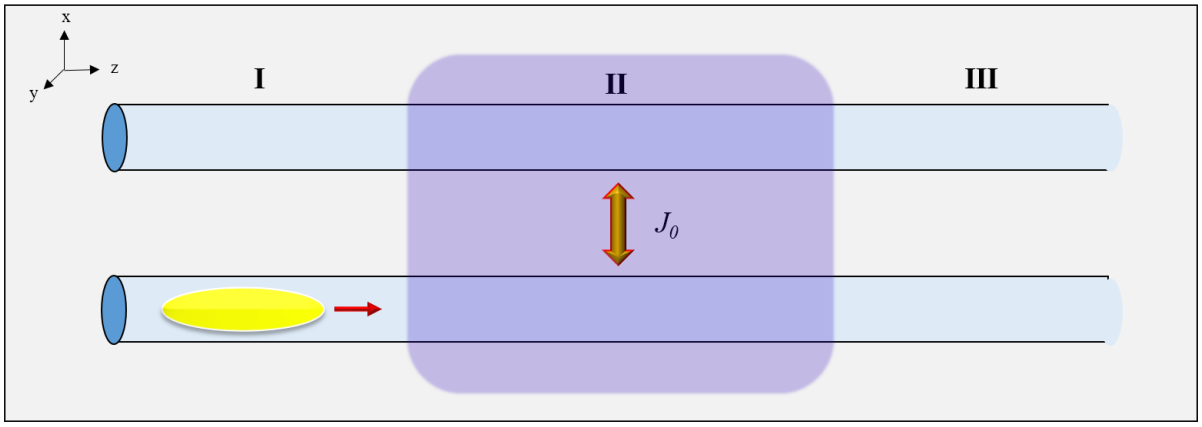

Figure 4.1: Schematic for spatially dependent coupling $J(z)$ setup with a moving bright soliton in Q1D tube along the z-axis. We have divided the space into three regions. In Region I and III, tubes are uncoupled with a negligible overlap in the transverse wave function, and Region I hosts the initial soliton moving with a velocity $+k_0$. Region II extends over a length 2δ in between where the tubes are coupled with strength J_0 which determines the dynamical regime of the system.

In this section, we describe the system with the space-dependent coupling term, $J(z)$. As discussed in the previous chapters, in order to modify the dynamical parameter Λ, we can either vary the interaction strength g or change the lattice parameters, like spacing b and depth V_0, to make J space-dependent. In this study, we choose for J to take the explicit form:

$$J(z) = \begin{cases} 0, & \text{if } |z| > \delta \\ J_0, & \text{if } |z| \leq \delta \end{cases} \tag{4.1}$$

where we consider a uniform inter-layer coupling J_0 between the tubes over a central region of length "2δ", as illustrated in (4.1). In 4.1.1, we point out certain imperfections that need to be considered in getting to the quasi-1D setup with $J(z)$.

4.1.1 Imperfections

We start with the same 3D GPE as before but now with the 2D lattice potential, $V(x, y, z)$, having its depth varying along the z-axis, such that, the transverse overlap of the Wannier states is larger inside the region II. Therefore, the 3D GPE is given by:

$$i\hbar\frac{\partial\Psi}{\partial t}(\mathbf{r},t) = \left(\frac{-\hbar^2}{2M}\boldsymbol{\nabla}^2 + V_{ol}(x,y,z) + g\left|\Psi(\mathbf{r},t)\right|^2\right)\Psi(\mathbf{r},t) \tag{4.2}$$

The potential now changes with z as

$$V_{ol}(x,y,z) = V_0(z)\ (\sin^2(kx) + \sin^2(ky)) \tag{4.3}$$

where $V_0(z)$ is reduced to induce a larger overlap inside the coupling region. This affects the Wannier bases as well, given by $w_i(x, y, z)$. We use the ansatz $\Psi(x, y, z, t) = w_1(x, y, z)\psi_1(z, t) + w_2(x, y, z)\psi_2(z, t)$ and simplify the 3D GPE in the same way as before, using the weak coupling approximations and finally arrive at dimensionless 1D GPE for ψ_1:

$$\begin{aligned} i\frac{\partial\psi_1}{\partial t} =& -\frac{1}{2}\frac{\partial^2\psi_1}{\partial z^2} \quad + g_{1D}(z)\left|\psi_1\right|^2\psi_1 \quad - J(z)\psi_2 \quad \text{(Coupled 1D GPE)} \\ & - \frac{1}{2}\psi_1\left[\int w_1^*\frac{\partial^2 w_1}{\partial z^2}dxdy\right] - \frac{1}{2}\psi_2\left[\int w_1^*\frac{\partial^2 w_2}{\partial z^2}dxdy\right] \\ & - \frac{\partial\psi_1}{\partial z}\left[\int w_1^*\frac{\partial w_1}{\partial z}dxdy\right] - \frac{\partial\psi_2}{\partial z}\left[\int w_1^*\frac{\partial w_2}{\partial z}dxdy\right] \\ & + \psi_1\left[\int w_1^*\left(V_0(z)(\sin^2(kx)+\sin^2(ky)) - \frac{1}{2}(\partial_x^2+\partial_y^2)\right)w_1\ dxdy\right] \\ & \text{(Corrections)} \end{aligned} \tag{4.4}$$

and similarly for ψ_2, where,

$$J(z) = -\int\left(-\frac{1}{2}w_1^*\left(\frac{\partial^2}{\partial x^2}+\frac{\partial^2}{\partial y^2}\right)w_2 + w_1^*\ V_{ol}(z)\ w_2\right)dxdy \tag{4.5}$$

Additional correctional terms are obtained as imperfections along with the original coupled 1D GPE, now with a spatially dependent $J(z)$. Here, we assume that these corrections do not significantly affect the characteristics of the dynamics. Alternatively, we can explore a method to induce this spatial dependence using the laser-controlled tunneling described in [30].

Now, we have the following coupled equations for our setup:

$$\begin{aligned} i\frac{\partial\psi_1}{\partial t} &= -\frac{1}{2}\frac{\partial^2\psi_1}{\partial z^2} + g_{1D}|\psi_1|^2\psi_1 - J(z)\psi_2 \\ i\frac{\partial\psi_2}{\partial t} &= -\frac{1}{2}\frac{\partial^2\psi_2}{\partial z^2} + g_{1D}|\psi_2|^2\psi_2 - J(z)\psi_1 \end{aligned} \tag{4.6}$$

We load a bright soliton in one of the tubes in region I, and provide it with an initial kick of velocity k_0 towards region II. We then examine its behavior as it enters region II and the effect of variation in J_0 and k_0 on the dynamics.

4.2 Results

We look at the dynamics of the coupled equations above in this section. Two distinct cases occur based on the value of J_0 or Λ. The dynamics are further divided into two scenarios based on k_0.

4.2.1 $\Lambda < \Lambda_c$

Upon entry, the population oscillates between the two tubes due to dominant tunneling as the soliton moves toward the right, as expected. Small excitations arise in each soliton's periphery during each cycle owing to the nonlinearity in the system. For Λ just below Λ_c, the oscillations are non-periodic and damped due to the competing interactions. A sudden

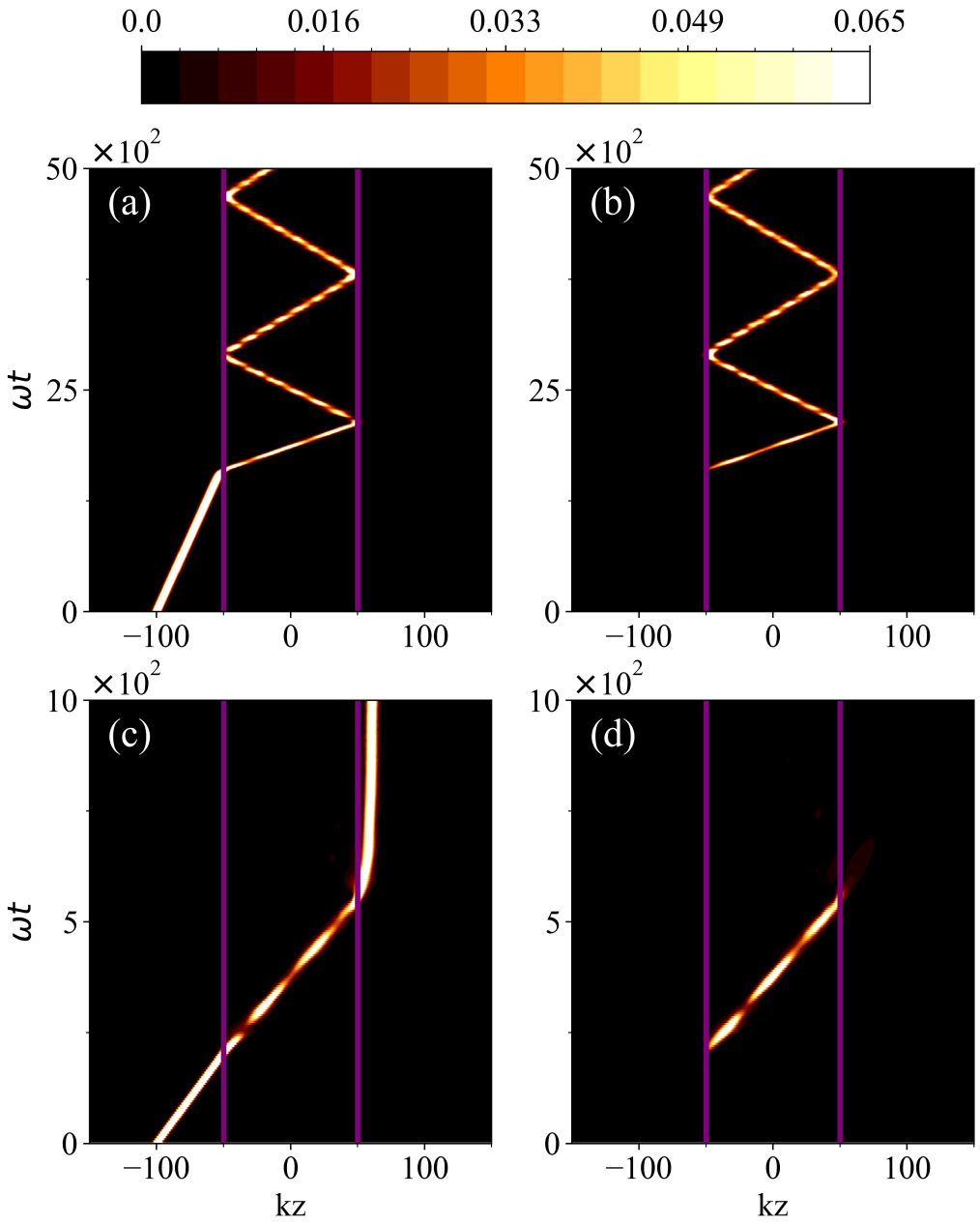

Figure 4.2: Dynamics of moving bright soliton encountering a region with coupling $\Lambda = 1.25 < \Lambda_c$, where $g_{1D} = -1$ and $\delta = 50$. Density evolution in each row corresponds to two coupled tubes and the colorbar on top sets the density scale for all. (a) and (b) for $k = +0.03$, soliton gets confined within region II in combination with performing population transfer oscillations around $p \approx 0$ and (c) and (d) for $k = +0.245$, soliton mass oscillates between the tubes when inside region II and escapes confinement into region III.

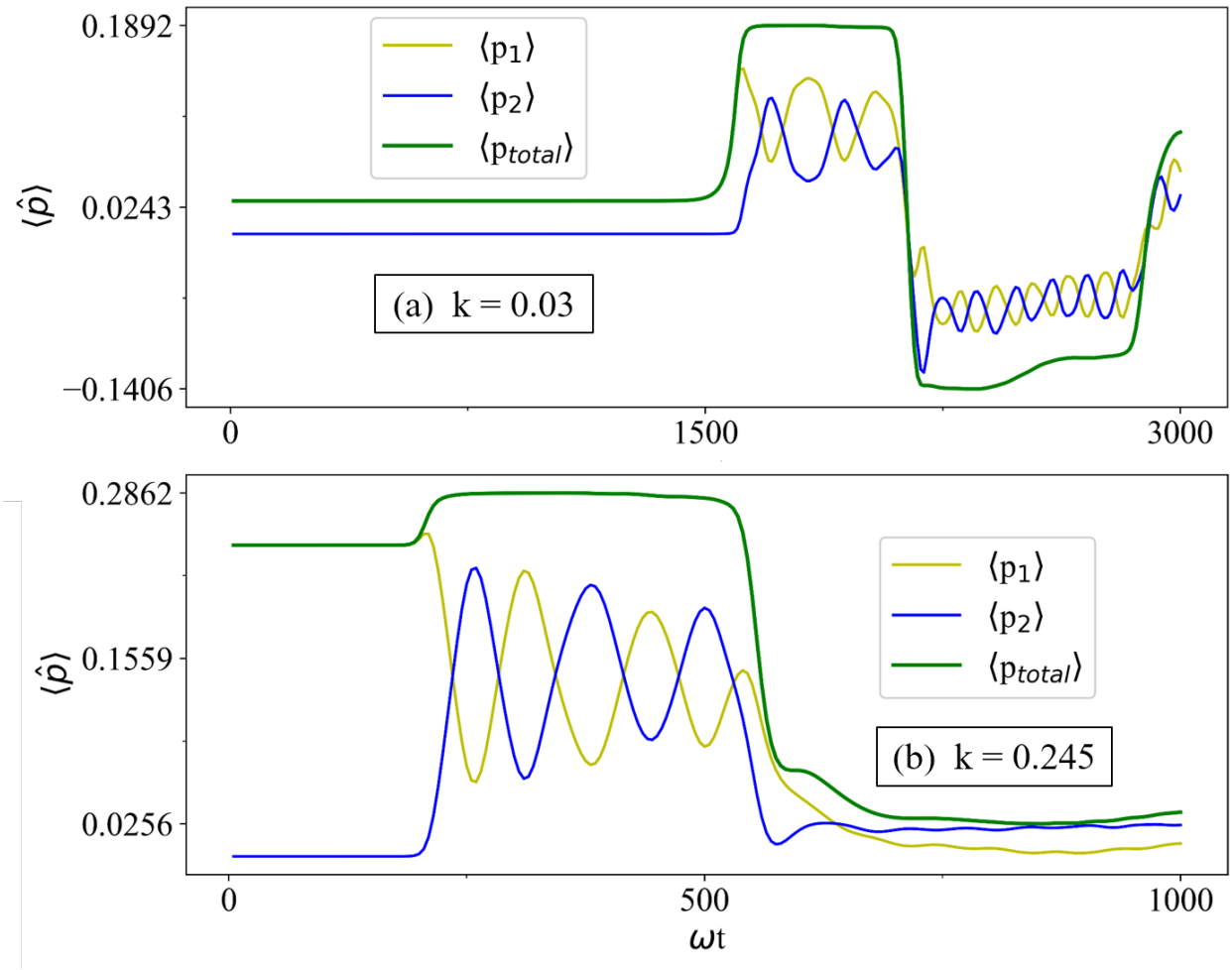

Figure 4.3: $\langle p_{total} \rangle$ vs time (red line) for $\Lambda = 1.25 < \Lambda_c$ case. See (a) for $k = +0.03$ and (b) for $k = +0.245$. We note the sudden rise and fall of $\langle p_{total} \rangle$ on encountering boundaries of region II accompanied by relatively stable evolution elsewhere, in both (a) and (b). $\langle p_1 \rangle$ and $\langle p_2 \rangle$ also show rapid changes at boundaries but oscillate about each other elsewhere in region II for both cases.

increase in the total momentum, $p_{total}(t)$, is observed here, as shown in (4.3). Depending on the initial velocity k_0, two distinct cases are described below for a fixed δ.

For $\Lambda < \Lambda_c$ and $k_0 = 0.03$, the soliton accelerates after entering region II, as the density tunnels back and forth between the layers generating small non-linear excitations in the process (see (a) and (b) in figure 4.2). On interacting with the region II boundary, the soliton in both tubes reflects back almost completely, leaving only the tiny excitations to pass through to region III. The condensate mass keeps on oscillating between the layers as it gets trapped inside region II. Similar behavior is observed as k_0 is increased over a large range.

For very large velocity scales above a critical velocity scale k_c, near $k_0 = 0.24$, large fractions of the soliton transmit out to region III and the remaining fraction reflects back (see (c) and (d) in figure 4.2). For $k_0 = 0.4$ or higher, the majority of the soliton passes through to region III. However, with smaller time scales and relatively low non-linearity due to large J_0, the soliton is unable to tunnel back to one of the tubes which would have led to a lower energy configuration. On emerging through to region III in this case, it continues to propagate without much dispersion with arbitrary fractions of the solitons in each layer. It should be noted that by varying δ, k_c also varies and so do the emergent soliton fractions at $k > k_c$. As a result, the average total mass fraction trapped inside region II shows a gradual drop near $k_0 \approx k_c$.

4.2.2 $\Lambda > \Lambda_c$

Once the soliton enters region II, a major fraction of the soliton stays self-trapped in the same layer due to dominant self-focusing attractive interactions, as expected, while a small fraction tunnels through to the other layer. Depending on how close Λ is to Λ_c, the fraction in each well varies. The total momentum, $p_{total}(t)$, of the two layers also shows a sudden increase upon entry to region II. Similarly, we now describe two cases based on k_0.

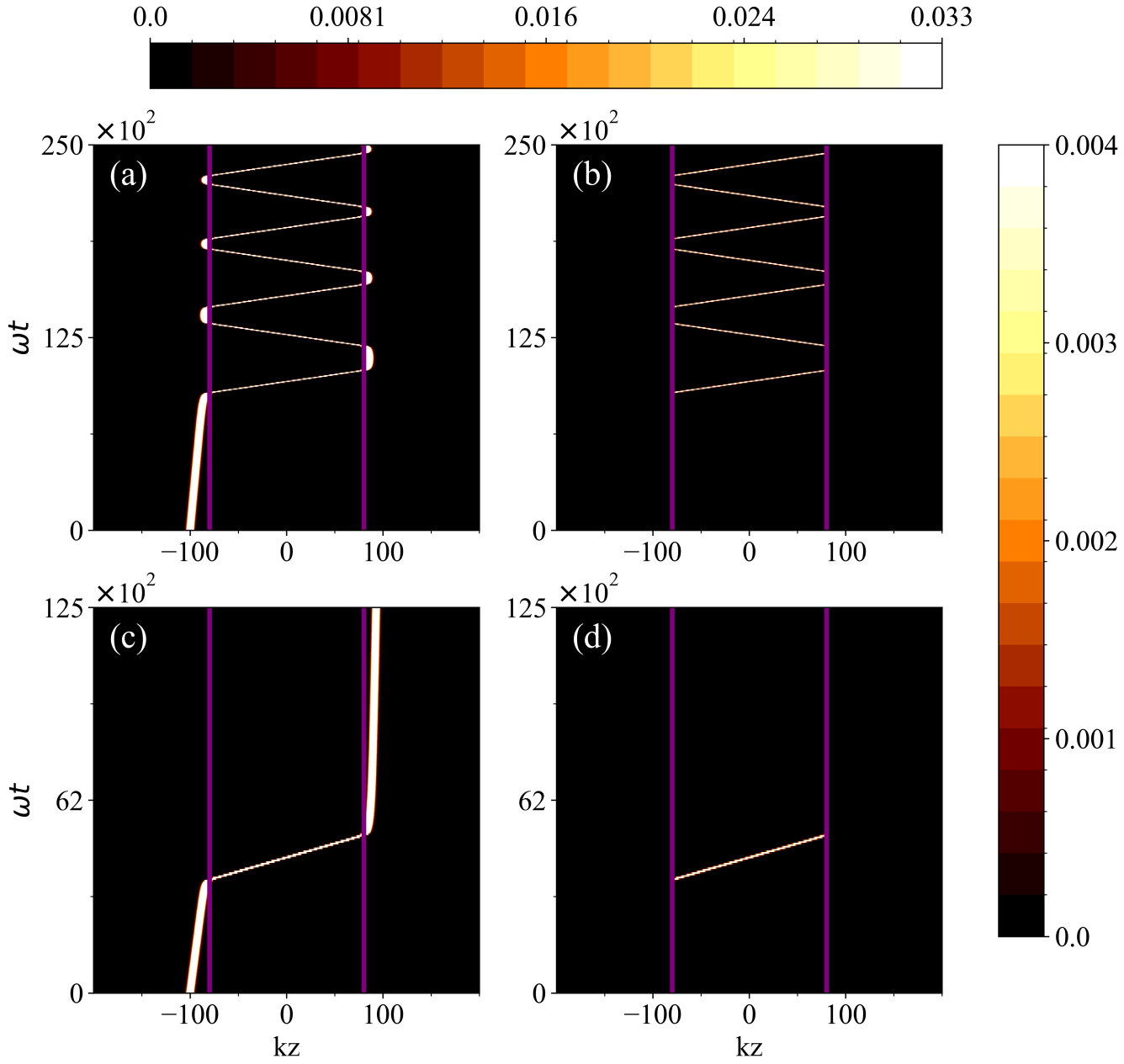

Figure 4.4: Dynamics of moving bright soliton encountering a region with coupling $\Lambda = 2.08 > \Lambda_c$, where $g_{1D} = -1$ and $\delta = 80$. Density evolution in each row corresponds to two coupled tubes. Colorbar on top sets the density scale for (a) and (c) and on the right sets a smaller density scale for (b) and (d). (a) and (b) for $k = +0.0015$, soliton gets confined within region II and self-trapped in tube (a). (c) and (d) for $k = +0.0042$, soliton is self-trapped when inside region II and escapes confinement into region III.

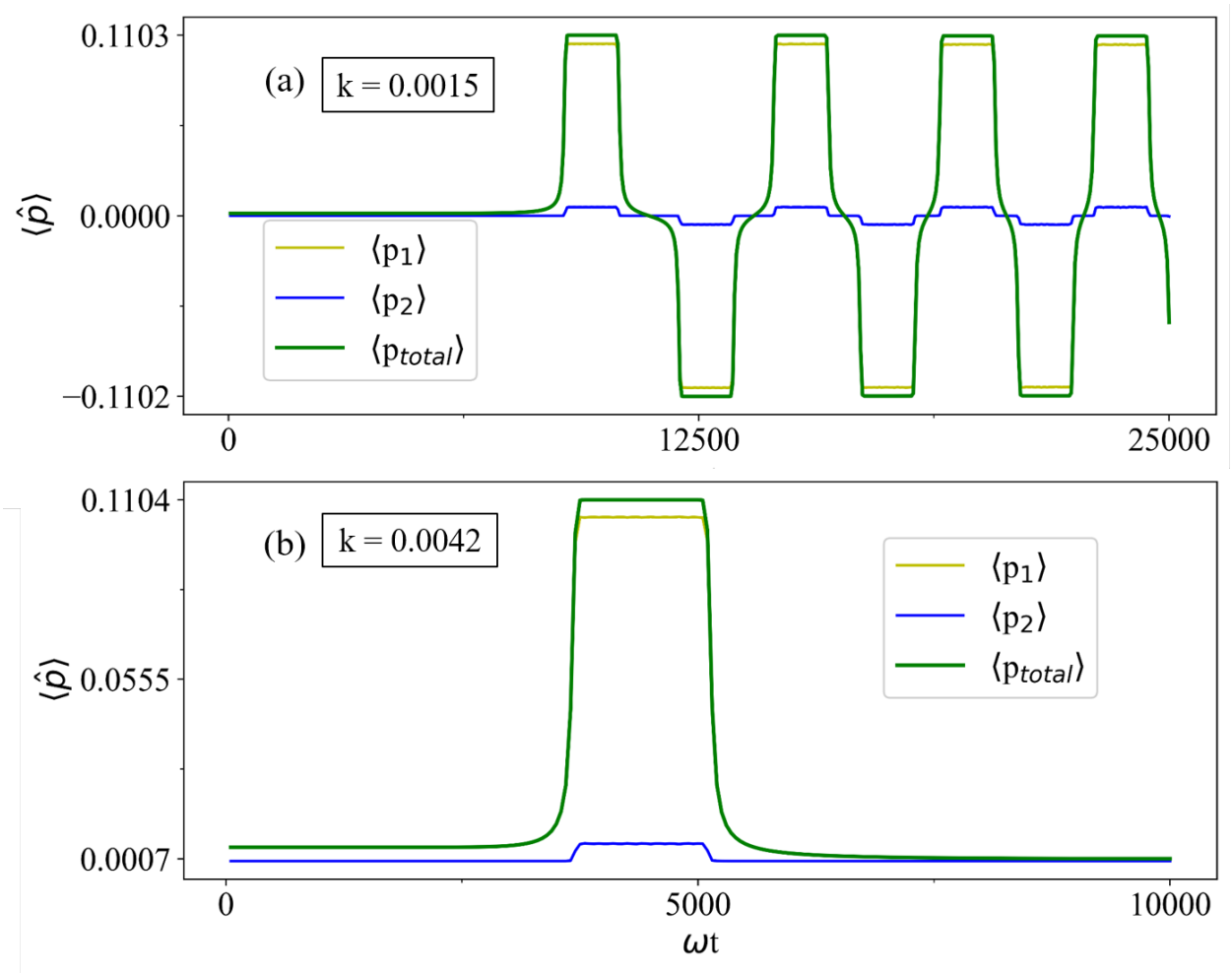

Figure 4.5: $\langle p_{total} \rangle$ vs time (red line) for $\Lambda = 2.08 > \Lambda_c$ case. See (a) for $k = +0.0015$ and (b) for $k = +0.0042$. Here also, we note the sudden rise and fall of $\langle p_{total} \rangle$ on encountering boundaries of region II in (a) and (b). $\langle p_1 \rangle$ and $\langle p_2 \rangle$ also show rapid changes at boundaries.

For a low velocity $k_0 = 0.03$ (see (c) and (d) in figure 4.4), on entry, the condensate stays self-trapped and splits into a minor and a major fraction, as discussed above. On approaching the boundary of region II at $z = +\delta$, the smaller fraction tunnels back to integrate with the larger part, and the condensate transfers back to one layer completely. While $p_{total}(t)$ suddenly increases during entry to region II, it shows a sharp decrease upon exiting region II (Figure 4.5). The soliton emerges outside nearly identical to the initial soliton, but with a different momentum.

As we lower the initial velocity k_0 for the same J_0, despite the dynamics being qualitatively identical, the emerging soliton records a trend of decreasing $p_{total}(t)$ exiting from the region II. Eventually, it reaches a critical velocity k_c, where its final $p_{total}(t)$ becomes nearly zero. For any further decrease in k_0, the sign of $p_{total}(t)$ changes at the boundary and the soliton reflects back into region II instead of passing through. Subsequently, it always reflects back on encountering the boundaries at $z = \pm\delta$ again and hence gets confined within region II (see (a) and (b) in figure 4.4). The average total mass fraction trapped inside region II shows a sudden drop near $k_0 \approx k_c$, below which the majority of the soliton fraction gets confined in region II, while still staying self-trapped within one of the tubes. For all $k_0 > k_c$, the soliton gets transmitted through to region III.

4.2.3 Dynamical Potential

We see that the condensate is confined within region II below a critical velocity k_c for values of Λ in both dynamical regimes. Corresponding to the critical transition observed in the dynamics when Λ crosses Λ_c, there is a sudden drop in the critical velocity required for the soliton to pass through. From this, it can be inferred that the effective trapping potential evolves dynamically with the system. To explore the relation between this "effective potential" and the dynamical regimes, we first look at the evolution of the total momentum. Evidently, linear momentum is not conserved because $J(z)$ breaks the translational invariance

of the Hamiltonian. We calculate an expression for the force on the overall condensate by taking the time derivative of $\langle p_{total}(t)\rangle$:

$$\frac{d\langle \hat{p}_{total}\rangle}{dt} = \int \left(\psi_1^* \left(\frac{\partial J(z)}{\partial z} \right) \psi_2 + \psi_2^* \left(\frac{\partial J(z)}{\partial z} \right) \psi_1 \right) dz, \tag{4.7}$$

This suggests that the condensate experiences a non-zero force at the boundary where $J(z)$ changes value and that it has a dependence on the wave functions as well. Using the Ehrenfest theorem, we get an insight into the nature of this potential:

$$\begin{aligned} \frac{d\langle \hat{p}\rangle}{dt} &= \left\langle -\frac{\partial V}{\partial x} \right\rangle \\ &= \int \left(\psi_1^* \left(\frac{\partial J(z)}{\partial z} \right) \psi_2 + \psi_2^* \left(\frac{\partial J(z)}{\partial z} \right) \psi_1 \right) dz, \end{aligned} \tag{4.8}$$

We use a variational approach in the next section to get an explicit expression for this effective potential in terms of dynamical variables and compare the resulting dynamics to numerical simulations of the GPE.

4.3 Variational Calculation

We divide this section into two parts based on the initial states and the number of variational parameters.

4.3.1 Symmteric Case

Owing to the complexity afforded to the Lagrangian by the off-diagonal term J and the moving solitons, we start with a symmetric initial state to simplify the calculations. We consider two identical GS bright solitons, one in each tube, in the central region II. Both the solitons are given an initial velocity $+k_0$ at initial time $t = 0$. Since no initial asymmetry

in mass or phase is allowed, no population transfer is expected. This allows us to assume a symmetric GS sech ansatz for our calculations, given by:

$$\psi_j = \frac{A}{\sqrt{2}} \operatorname{sech}\left(\frac{z - z_0}{l}\right) \exp\left(+i\alpha(z - z_0) + i\phi\right) \tag{4.9}$$

where A (real amplitude), z_0 (center of mass), l (width), ϕ (phase), and α (slope) are constrained to be identical for both wavefunctions during the dynamics. From (3.4), the Lagrangian is given by:

$$\begin{aligned} L(t) = \int_{-\infty}^{\infty} \sum_{j=1,2} \left[\frac{i}{2}\left(\psi_j^* \frac{\partial \psi_j}{\partial t} - \psi_j \frac{\partial \psi_j^*}{\partial t}\right) - \frac{1}{2}\left|\frac{\partial \psi_j}{\partial z}\right|^2 - \frac{g}{2}\left|\psi_j\right|^4 \right] dz \\ + \int_{-\delta}^{\delta} \left[J_0 \left(\psi_1^* \psi_2 + \psi_1 \psi_2^*\right) \right] dz \end{aligned} \tag{4.10}$$

Inserting the variational ansatz in the above and evaluating the Lagrangian, we get

$$L(t) = 2A^2 l(\alpha \dot{z_0} - \dot{\phi}) - A^2 l\alpha^2 - \frac{A^2}{3l} + \frac{gA^4 l}{3} + J_0 A^2 l \left[\tanh\left(\frac{z_0 + \delta}{l}\right) - \tanh\left(\frac{z_0 - \delta}{l}\right)\right] \tag{4.11}$$

From the Euler-Lagrange equations for ϕ and α, we get $\dot{z_0} = \alpha$ and conservation of total mass, $2A^2 l = N_T$. Rewriting the Lagrangian,

$$L(t) = N_T(\alpha \dot{z_0} - \dot{\phi}) - \frac{N_T}{2}\alpha^2 - \frac{N_T}{6l^2} - \frac{gN_T^2}{12l} + \frac{J_0 N_T}{2} \left[\tanh\left(\frac{z_0 + \delta}{l}\right) - \tanh\left(\frac{z_0 - \delta}{l}\right)\right] \tag{4.12}$$

From the E-L equations for z_0 and l, we get the following coupled equations for their time evolution:

$$\begin{aligned} \ddot{z_0} &= \frac{J_0}{2l}\left[\operatorname{sech}^2\left(\frac{z_0 + \delta}{l}\right) - \operatorname{sech}^2\left(\frac{z_0 - \delta}{l}\right)\right] \\ \frac{1}{l} &= \frac{3J_0}{2}\left[(z_0 + \delta)\operatorname{sech}^2\left(\frac{z_0 + \delta}{l}\right) - (z_0 - \delta)\operatorname{sech}^2\left(\frac{z_0 - \delta}{l}\right)\right] - \frac{gN_T}{4} \end{aligned} \tag{4.13}$$

We numerically simulate these two coupled differential equations. Dynamical trapping is observed depending on the initial value of α_0 and J_0. Figures (4.6) and (4.7) give the evolution of the COM $z_0(t)$ and width $l(t)$ for $\Lambda = 1.25 < \Lambda_c$ and $\Lambda = 6.25 > \Lambda_c$ respectively. For each value of J_0, we find a α_0 to ensure confinement within the central region and a critical α_c required for it to escape confinement. Evolution of $l(t)$ for the trapped case shows that, for a small $\alpha(0)$, the width of the soliton varies negligibly at the boundaries, where it squeezes, and regains its width as it reflects back inside the region II.

The effective potential $V_{eff}(z_0)$ can be determined by integrating the force acting on the COM coordinate, $\ddot{z}_0$, through Eq.(4.13). Assuming $l(t)$ varies negligibly at the borders, the expression for $V_{eff}(z_0)$ can be written as:

$$V_{eff}(z_0) = -\int^{z_0} F(z)dz \;=\; \frac{J_0}{2}\left[\tanh\left(\frac{z_0-\delta}{l}\right) - \tanh\left(\frac{z_0+\delta}{l}\right)\right] \tag{4.14}$$

For a fixed width l, $V_{eff}(z_0)$ is shaped like a smooth well centered at $z = 0$. The depth of the well is proportional to J_0 and the slope at the borders depends inversely on the width of the soliton. Figure (4.8) shows $V_{eff}(z_0)$ vs z_0, which describes the nature of the confining potential faced by the soliton at its center of mass. Starting from $z = 0$, as $z_0(t)$ approaches $z = \pm\delta$ during evolution, it encounters a rising restorative force towards the center $z = 0$ as the potential hill gets steeper. As we go past $z = \pm\delta$, the force starts to reduce as the potential hill begins to plateau. This is analogous to a ball thrown up a hill from inside a valley, with the hill is shaped like tanh. Given enough kinetic energy from the throw, the ball climbs up the hill, reaches the plateau, and continues to roll along with a reduced velocity. If the initial kinetic energy is not sufficient to make the climb, the ball rolls back inside and oscillates back and forth inside the valley. Consequently, if the initial kinetic energy is exactly $J_0/2$, the ball must come to an eventual stop at $z_0 \to \infty$. A key difference to point out in our system is that the slope of the potential hill depends on the $l(t)$ of the soliton, which is a dynamic parameter.

However, it should be noted that since the norms and phases are constrained to be the

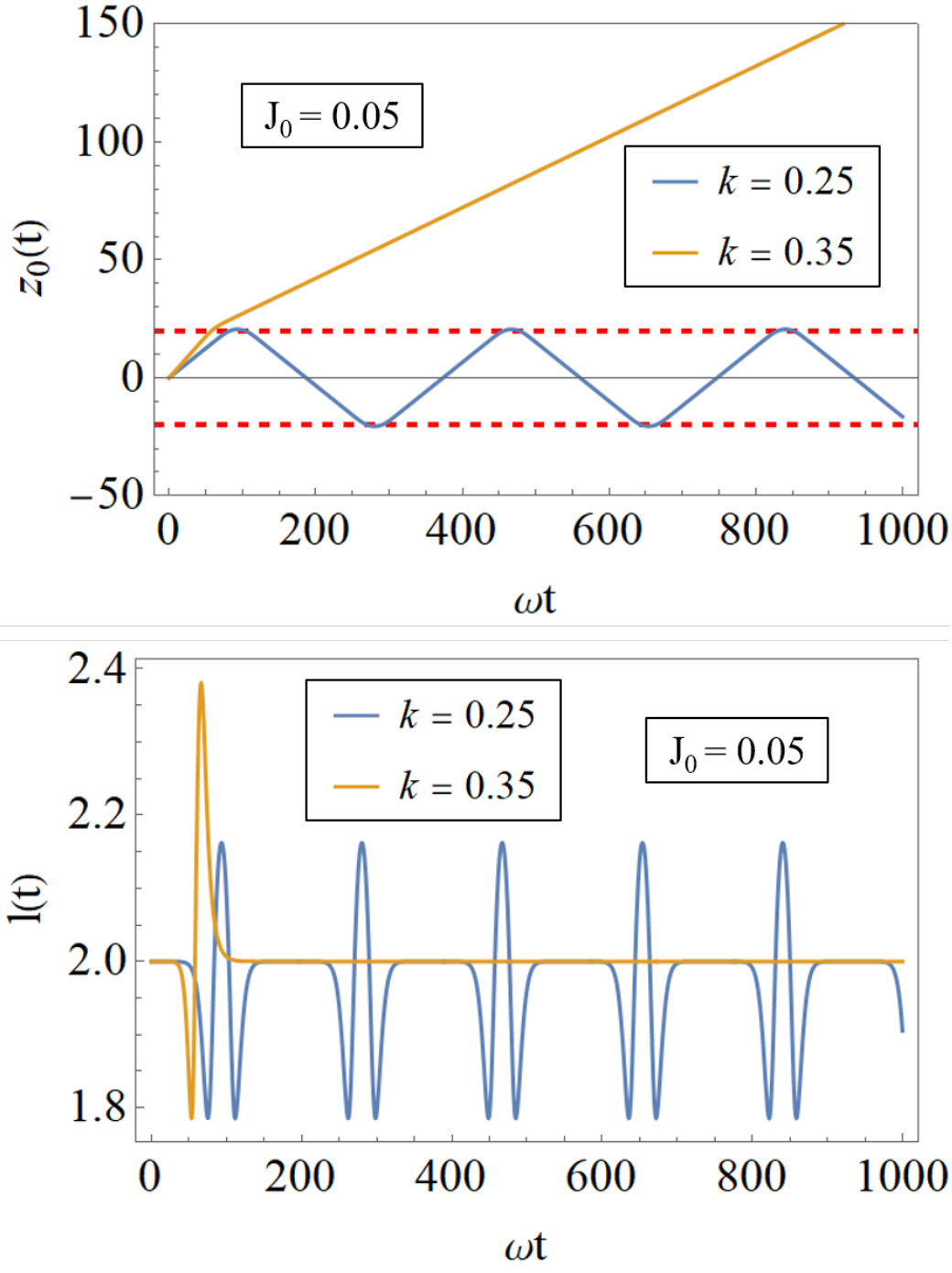

Figure 4.6: Time evolution of variational parameters for $\Lambda = 1.25 < \Lambda_c$: (a) $z_0(t)$ and (b) $l(t)$ for two identical bright solitons in region II kicked with velocity k. Critical velocity to escape confinement in region II lies between $0.25 < k_c < 0.35$.

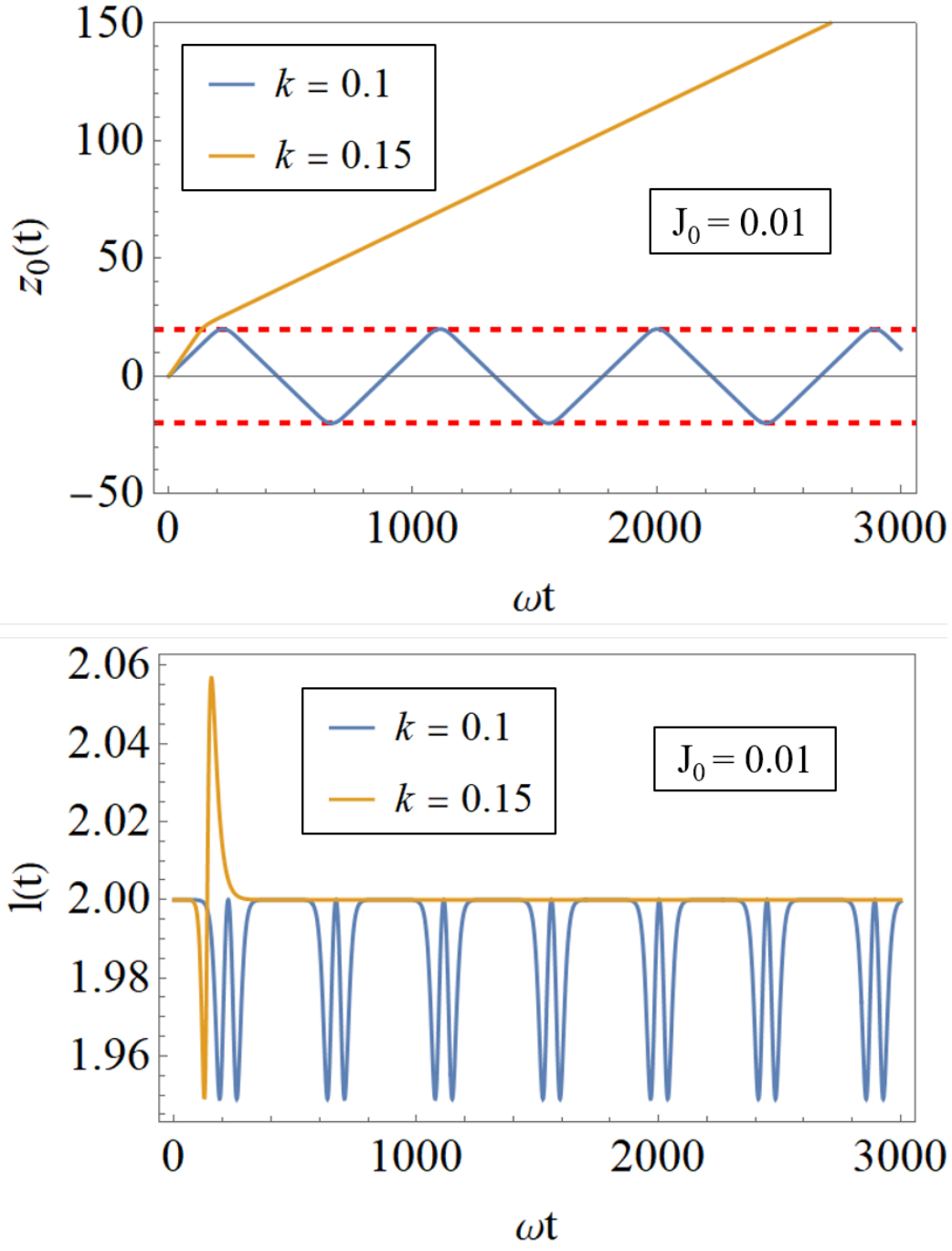

Figure 4.7: Time evolution of variational parameters for $\Lambda = 6.25 > \Lambda_c$: (a) $z_0(t)$ and (b) $l(t)$ for two identical bright solitons in region II kicked with velocity k. Critical velocity to escape confinement in region II lies between $0.1 < k_c < 0.15$.

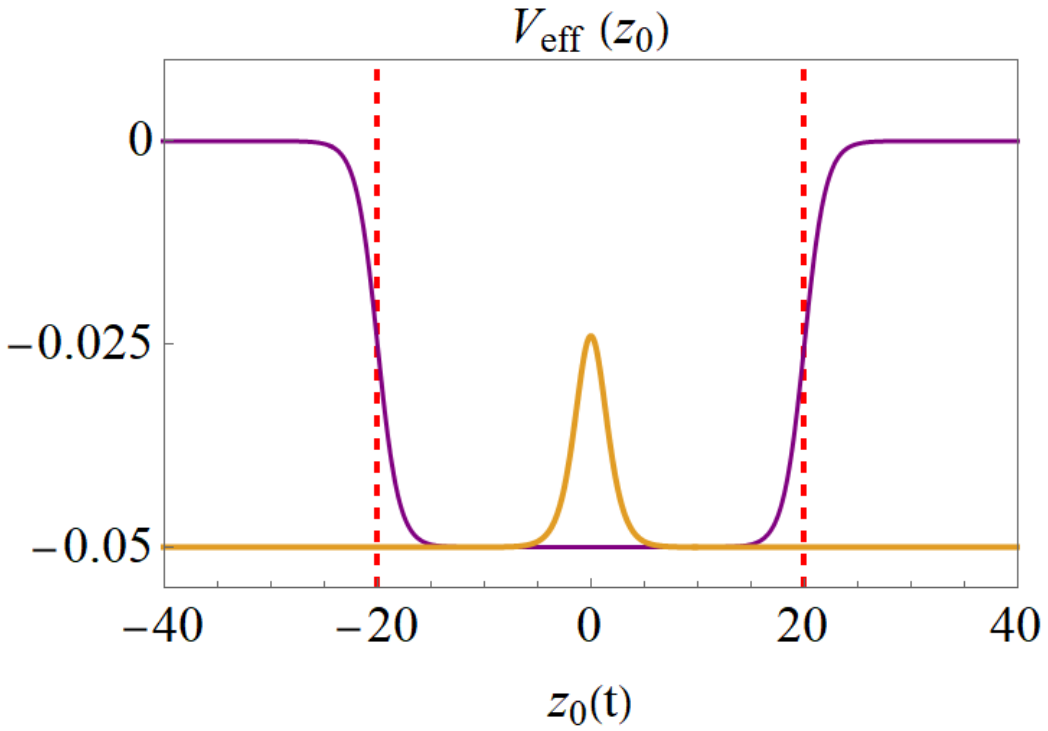

Figure 4.8: Effective Dynamical Potential V_{eff} vs z_0 (purple line) for a pair of identical bright solitons inside coupling region. Dashed vertical line denotes the region boundaries at $\pm\delta$ and the yellow line represents bright solitons inside it.

same, the effect of the critical transition between self-trapping and switching regimes cannot be captured through this variational calculation.

4.3.2 Asymmetric Case

Here, we introduce a scope for asymmetry in the variational ansatz to allow for more complex dynamics but use a normalized gaussian waveform to simplify calculations. It is given by:

$$\psi_j = \frac{A_j}{\pi^{1/4}} \exp\left(-\frac{(z-z_0)^2}{2l_j^2} + i\alpha(z-z_0) + i\phi_j \right) \tag{4.15}$$

where the parameters are the same as before but have been indexed with j for the two tubes. Note that z_0 and α are still taken to be identical.

After proceeding with similar calculations and rewriting $L(t)$ in terms of $N_T = A_1^2 l_1 + A_2^2 l_2 = N_1 + N_2$, $R = N_1 - N_2$, $\phi = \phi_1 - \phi_2$, $\theta = \phi_1 + \phi_2$, l_1, l_2 and z_0:

$$\begin{aligned} L(t) =& \frac{N_T}{2}\dot{z_0}^2 - \frac{R\dot{\phi}}{2} - \frac{1}{8}\left(\frac{(R+N_T)}{l_1^2} + \frac{(N_T-R)}{l_2^2}\right) - \frac{g}{2\sqrt{2\pi}}\left(\frac{(R+N_T)^2}{l_1} + \frac{(N_T-R)^2}{l_2}\right) \\ &+ \frac{J_0\cos(\phi)}{2}\sqrt{\frac{2l_1l_2(N_T^2-R^2)}{l_1^2+l_2^2}} \times \left[\operatorname{erf}\left(\frac{\sqrt{l_1^2+l_2^2}}{\sqrt{2}l_1l_2}(z_0+d)\right) - \operatorname{erf}\left(\frac{\sqrt{l_1^2+l_2^2}}{\sqrt{2}l_1l_2}(z_0-d)\right)\right] \end{aligned} \tag{4.16}$$

Note that θ is a cyclic coordinate and hence conserved throughout the dynamics and can be safely ignored. We now use the E-L equations and get the 5 coupled differential equations, of which we state:

For ϕ:

$$\dot{R} = J_0\sin(\phi)\sqrt{\frac{2l_1l_2(N_T^2-R^2)}{l_1^2+l_2^2}}\left[\operatorname{erf}\left(\frac{\sqrt{l_1^2+l_2^2}}{\sqrt{2}l_1l_2}(z_0+d)\right) - \operatorname{erf}\left(\frac{\sqrt{l_1^2+l_2^2}}{\sqrt{2}l_1l_2}(z_0-d)\right)\right] \tag{4.17}$$

For R:

$$\frac{\dot{\phi}}{2} = \frac{1}{8}\left(\frac{1}{l_2^2} - \frac{1}{l_1^2}\right) - \frac{g}{\sqrt{2\pi}}\left[R\left(\frac{1}{l_1} + \frac{1}{l_2}\right) + N_T\left(\frac{1}{l_1} - \frac{1}{l_2}\right)\right] - \frac{J_0\cos(\phi)}{2}\sqrt{\frac{2l_1l_2}{l_1^2+l_2^2}}\frac{R}{\sqrt{N_t^2-R^2}}\left[\text{erf}\left(\frac{\sqrt{l_1^2+l_2^2}}{\sqrt{2}l_1l_2}(z_0+d)\right) - \text{erf}\left(\frac{\sqrt{l_1^2+l_2^2}}{\sqrt{2}l_1l_2}(z_0-d)\right)\right] \tag{4.18}$$

For z_0:

$$\ddot{z_0} = \frac{J_0\cos(\phi)}{N_T}\sqrt{\frac{N_T^2-R^2}{\pi l_1l_2}}\left[\exp\left(-\frac{(z_0+d)^2(l_1^2+l_2^2)}{2l_1^2l_2^2}\right) - \exp\left(-\frac{(z_0-d)^2(l_1^2+l_2^2)}{2l_1^2l_2^2}\right)\right] \tag{4.19}$$

While numerical simulations of these five coupled equations should yield dynamics close to the original GPE, we utilize these expressions to get a more qualitative feel for the effective potential. From (4.19), it can be seen that $\ddot{z_0}$ is proportional to J_0 which decides the maximum depth of the valley in V_{eff}. It is also proportional to $\cos(\phi)$ and $\sqrt{N_T^2-R^2}$. As can be seen, $\sqrt{N_T^2-R^2}$ is maximum at $R(t) = 0$ and reduces like an inverse parabola as R goes away from 0. For the switching case, $\langle R(t)\rangle \approx 0$, which implies that V_{eff} is deeper on average compared to the self-trapped case, where $\langle R(t)\rangle \neq 0$. This explains the rapid climb seen in the critical velocity k_c (figure) required to escape region II, as we cross from one dynamical regime to the other.

From this chapter, we conclude that the introduction of spatial dependence in coupling J of matter-wave bright solitons leads to their dynamical confinement inside the coupling region critically depending on the velocity k_0. The dynamical regimes based on Λ studied previously lead to qualitatively different cases of confinement. On further investigation using variational methods, we derive the explicit form of the effective trapping potential which is shaped like a valley. We emphasize the importance of the localization phenomenon observed in this setup and its possible implications on the controllability of solitons in optical lattices.

Chapter 5

Conclusion

In this thesis, we studied the dynamics of weakly coupled matter-wave bright solitons in a 2D optical lattice. We first looked at the dynamics of two GS bright solitons in Q1D tubes as a function of the critical parameter Λ. We see that when an initial asymmetry is provided in the overall phase or population of the two solitons, non-trivial dynamics are triggered and a critical transition is observed between two dynamical regimes based on Λ. For $\Lambda < \Lambda_c$, coherent Josephson-like oscillations with a frequency of $\omega_R \approx 2J$ are seen in the population difference p around zero. As the interactions are increased, $\Lambda \approx \Lambda_c$, oscillations in p, while still around zero, become increasingly anharmonic before transitioning to the macroscopically quantum self-trapped (MQST) regime for $\Lambda > \Lambda_c$, where p oscillates about some $p \neq 0$, and the soliton gets self-locked in one of the tubes. We find that Λ_c depends on the initial state p_0 and ϕ_0, and increases with the extent of initial asymmetry.

We then study the dynamics of moving bright soliton(s) when the linear coupling is turned on for only a finite region in the two tubes. We observe two cases of dynamical confinement in the region depending on the velocity k for $\Lambda < \Lambda_c$ and $\Lambda > \Lambda_c$. In the former case, the soliton gets confined inside the region while the population oscillates for all velocities below a large k_c. In the latter case, the soliton gets confined only below a very small k_c and stays

self-trapped in one tube. Using variational calculations, an effective dynamical potential for trapping is derived which is shaped like a smooth well, with its depth and slope varying with the solitons' dynamics.

Bibliography

[1] Satyendra Nath Bose. Plancks gesetz und lichtquantenhypothese. 1924.

[2] Albert Einstein. Quantentheorie des einatomigen idealen gases. zweite abhandlung. *Albert Einstein: Akademie-Vorträge: Sitzungsberichte der Preußischen Akademie der Wissenschaften 1914–1932*, pages 245–257, 2005.

[3] Mike H Anderson, Jason R Ensher, Michael R Matthews, Carl E Wieman, and Eric A Cornell. Observation of bose-einstein condensation in a dilute atomic vapor. *science*, 269(5221):198–201, 1995.

[4] Kendall B Davis, M-O Mewes, Michael R Andrews, Nicolaas J van Druten, Dallin S Durfee, DM Kurn, and Wolfgang Ketterle. Bose-einstein condensation in a gas of sodium atoms. *Physical review letters*, 75(22):3969, 1995.

[5] Cl C Bradley, CA Sackett, JJ Tollett, and Randall G Hulet. Evidence of bose-einstein condensation in an atomic gas with attractive interactions. *Physical review letters*, 75(9):1687, 1995.

[6] Panayotis G Kevrekidis, Dimitri J Frantzeskakis, and Ricardo Carretero-González. *Emergent nonlinear phenomena in Bose-Einstein condensates: theory and experiment*, volume 45. Springer, 2008.

[7] Luigi Amico, Malcolm Boshier, Gerhard Birkl, Anna Minguzzi, Christian Miniatura, L-C Kwek, Davit Aghamalyan, Veronica Ahufinger, Dana Anderson, Natan Andrei, et al. Roadmap on atomtronics: State of the art and perspective. *AVS Quantum Science*, 3(3):039201, 2021.

[8] Philip W Anderson. Absence of diffusion in certain random lattices. *Physical review*, 109(5):1492, 1958.

[9] André Eckardt. Colloquium: Atomic quantum gases in periodically driven optical lattices. *Reviews of Modern Physics*, 89(1):011004, 2017.

[10] Oliver Morsch and Markus Oberthaler. Dynamics of bose-einstein condensates in optical lattices. *Reviews of modern physics*, 78(1):179, 2006.

[11] Rudolf Grimm, Matthias Weidemüller, and Yurii B Ovchinnikov. Optical dipole traps for neutral atoms. In *Advances in atomic, molecular, and optical physics*, volume 42, pages 95–170. Elsevier, 2000.

[12] GL Alfimov, PG Kevrekidis, VV Konotop, and M Salerno. Wannier functions analysis of the nonlinear schrödinger equation with a periodic potential. *Physical Review E*, 66(4):046608, 2002.

[13] ML Chiofalo, M Polini, and MP Tosi. Collective excitations of a periodic bose condensate in the wannier representation. *The European Physical Journal D-Atomic, Molecular, Optical and Plasma Physics*, 11:371–378, 2000.

[14] Nicola Marzari, Arash A Mostofi, Jonathan R Yates, Ivo Souza, and David Vanderbilt. Maximally localized wannier functions: Theory and applications. *Reviews of Modern Physics*, 84(4):1419, 2012.

[15] Andrea Trombettoni and Augusto Smerzi. Discrete solitons and breathers with dilute bose-einstein condensates. *Physical Review Letters*, 86(11):2353, 2001.

[16] L. Pitaevskii and S. Stringari. *Bose-Einstein Condensation and Superfluidity*. International Series of Monographs on Physics. OUP Oxford, 2016.

[17] Christopher J Pethick and Henrik Smith. *Bose–Einstein condensation in dilute gases*. Cambridge university press, 2008.

[18] CM Savage, NP Robins, and JJ Hope. Bose-einstein condensate collapse: A comparison between theory and experiment. *Physical Review A*, 67(1):014304, 2003.

[19] Masahito Ueda and Kerson Huang. Fate of a bose-einstein condensate with an attractive interaction. *Physical Review A*, 60(4):3317, 1999.

[20] Jordan M Gerton, Dmitry Strekalov, Ionut Prodan, and Randall G Hulet. Direct observation of growth and collapse of a bose–einstein condensate with attractive interactions. *Nature*, 408(6813):692–695, 2000.

[21] Elizabeth A Donley, Neil R Claussen, Simon L Cornish, Jacob L Roberts, Eric A Cornell, and Carl E Wieman. Dynamics of collapsing and exploding bose–einstein condensates. *Nature*, 412(6844):295–299, 2001.

[22] A Gammal, T Frederico, and Lauro Tomio. Critical number of atoms for attractive bose-einstein condensates with cylindrically symmetrical traps. *Physical Review A*, 64(5):055602, 2001.

[23] Michael W Jack and Makoto Yamashita. Bose-hubbard model with attractive interactions. *Physical Review A*, 71(2):023610, 2005.

[24] Luca Barbiero and Luca Salasnich. Quantum bright solitons in a quasi-one-dimensional optical lattice. *Physical Review A*, 89(6):063605, 2014.

[25] Piero Naldesi, Juan Polo Gomez, Boris Malomed, Maxim Olshanii, Anna Minguzzi, and Luigi Amico. Rise and fall of a bright soliton in an optical lattice. *Physical Review Letters*, 122(5):053001, 2019.

[26] Srikanth Raghavan, Augusto Smerzi, Stefano Fantoni, and SR Shenoy. Coherent oscillations between two weakly coupled bose-einstein condensates: Josephson effects, π oscillations, and macroscopic quantum self-trapping. *Physical Review A*, 59(1):620, 1999.

[27] Augusto Smerzi, Stefano Fantoni, Stefano Giovanazzi, and SR Shenoy. Quantum coherent atomic tunneling between two trapped bose-einstein condensates. *Physical Review Letters*, 79(25):4950, 1997.

[28] S Raghavan and GP Agrawal. Switching and self-trapping dynamics of bose-einstein solitons. *Journal of Modern Optics*, 47(7):1155–1169, 2000.

[29] Viet Hung Nguyen, Ignac Bugar, Mattia Longobucco, Ryszard Buczyński, Boris A Malomed, Marek Trippenbach, et al. Reversible ultrafast soliton switching in dual-core highly nonlinear optical fibers. *Optics Letters*, 45(18):5221–5224, 2020.

[30] Quentin Beaufils, Gunnar Tackmann, Xiaolong Wang, Bruno Pelle, Sophie Pelisson, Peter Wolf, and F Pereira Dos Santos. Laser controlled tunneling in a vertical optical lattice. *Physical Review Letters*, 106(21):213002, 2011.